EXPERIMENTAL AND ANALYTICAL PERFORMANCE ASSESSMENT OF A WIND TURBINE

by

Burak Bağırgan

B.S., Civil Engineering, Boğaziçi University, 2018

Submitted to the Institute for Graduate Studies in
Science and Engineering in partial fulfillment of
the requirements for the degree of
Master of Science

Graduate Program in Civil Engineering

Boğaziçi University

2020

ACKNOWLEDGEMENTS

I would like to express my great gratitude to my supervisor Professor Serdar Soyöz for his precious guidance, helpful advices and great support throughout this work. It was my pleasure to be included in his research group and benefit from his extensive knowledge and experience. I also want to express my sincere thanks to him for his kind and student-friendly attitude which enables us to have good communication and find solutions to any problem easily.

Also, I would like to thank to Professor Hilmi Luş and Associate Professor Ufuk Yazgan for accepting to be my thesis examination committee. I am thankful to them for their knowledgeable comments and advices.

I would also like to thank Professor Emre Otay, Onur Akagündüz, Soner Melih Kural and Hüseyin Obuz for their valuable helps in the site related problems of the wind turbine.

I would also like to pass my thanks to teaching assistants Emre Aytulun, Oğuz Şenkardeşler and Semih Gönen for their friendly attitude against my theoretical questions and helpful supports in the development of the finite element model.

I would also like to extend my thanks to my project mates Behrouz Badrkhani and Serap Hanbay for the cooperation and their instructive helps during this study.

Finally, I would like to express my deep gratitude to my girlfriend Volga and my family for their priceless support and continuous encouragement during my educational life. I would not be able to come through this difficult process successfully without their valuable supports.

ABSTRACT

EXPERIMENTAL AND ANALYTICAL PERFORMANCE ASSESSMENT OF A WIND TURBINE

In this study, the performance assessment of the wind turbine in the Sarıtepe Campus of the Boğaziçi University under wind and seismic loadings is performed. For this purpose, the finite element model of the wind turbine is developed in SAP2000 software. In the model, the foundation is also included to consider the soil flexibility on dynamic properties. The soil around piles is modeled with soil springs and the stiffnesses of these springs are determined according to the API guideline. Then, FEM updating is performed with two parameters which are steel Young's modulus and soil spring coefficient percentage. In the development of the error function used in the FEM updating process, natural frequencies and mode shapes of the first three modes are used. Then, a nonlinear model of the wind turbine considering the soil flexibility is developed in ANSYS software and pushover analysis is performed. The influence of considering dead load and initial imperfection is also investigated in the pushover analysis. Then, demand and capacity curves are compared, and performance point is obtained. Seismic fragility analysis considering wind load action of various mean wind speeds is performed with 11 earthquake records selected according to the design spectrum. Then, the resonance phenomenon is investigated to see whether the wind turbine experiences an additional excitation because of resonance but results show that additional excitation is not seen due to resonance effect. Finally, the theoretical buckling capacity of the wind turbine is calculated according to two different references and it is seen that analytical calculations give reasonable buckling capacities.

ÖZET

BİR RÜZGAR TÜRBİNİNİN DENEYSEL VE ANALİTİK PERFORMANS DEĞERLENDİRMESİ

Bu çalışmada, Boğaziçi Üniversitesi Sarıtepe Kampüsü'nde bulunan rüzgar türbininin, rüzgar ve sismik yükler altındaki performans değerlendirmesi yapılmıştır. Bu amaçla, rüzgar türbininin sonlu elemanlar modeli SAP2000 yazılımında geliştirilmiştir. Bu modelde, zemin esnekliğinin yapının dinamik özellikleri üzerindeki etkisini hesaba katmak için yapının temeli de modele dahil edilmiştir. Kazıklarının etrafındaki zemin, zemin yaylarıyla modellenmiştir ve bu yayların rijitlik değerleri API kılavuzuna göre belirlenmiştir. Daha sonra, sonlu eleman modeli (SEM) güncellemesi, çeliğin Young's modülü ve zemin yayları rijitlik katsayısı yüzdesi olmak üzere iki parametre ile gerçekleştirilmiştir. SEM güncelleme işleminde kullanılan hata fonksiyonunda, ilk üç modun doğal frekans ve mod şekilleri kullanılmıştır. Daha sonra, rüzgar türbininin yapı-zemin etkileşimini hesaba katan doğrusal olmayan sonlu eleman modeli ANSYS yazılımında oluşturulmuş ve itme analizi yapılmıştır. Ölü yük ve başlangıç kusurunun itme analizi üzerindeki etkisi araştırılmıştır. Daha sonra, talep ve kapasite eğrileri karşılaştırılmış ve performans noktası elde edilmiştir. Ardından, tasarım spektrumuna göre seçilen 11 deprem kaydı ile çeşitli ortalama rüzgar hızlarına sahip rüzgar yükleri hesaba katılarak sismik kırılganlık analizi yapılmıştır. Daha sonra, rüzgar türbininin rezonans etkisiyle ilave bir uyarıya maruz kalıp kalmadığı araştırılmış ancak rezonans nedeniyle ilave bir etkinin olmadığı gözlemlenmiştir. Son olarak, rüzgar türbininin teorik burkulma kapasitesi iki farklı referansa göre hesaplanmış ve analitik hesapların makul kapasite değerleri sağladığı görülmüştür.

TABLE OF CONTENTS

ACKNOWLEDGEMENTS . . . iii
ABSTRACT . . . iv
ÖZET . . . v
LIST OF FIGURES . . . viii
LIST OF TABLES . . . xi
LIST OF SYMBOLS . . . xiii
LIST OF ACRONYMS/ABBREVIATIONS . . . xvi
1. INTRODUCTION . . . 1
1.1. Overview . . . 1
1.2. Objective . . . 2
1.3. Literature Review . . . 3
1.4. Scope . . . 16
2. FINITE ELEMENT MODELING . . . 18
2.1. Tower, Foundation and Soil Details . . . 18
2.2. Development of the Finite Element Model . . . 22
2.2.1. *p-y* Curves . . . 24
2.2.1.1. *p-y* Curve for Sand Layer . . . 24
2.2.1.2. *p-y* Curve for Clay Layer . . . 28
2.2.2. *t-z* Curves . . . 29
2.2.2.1. *t-z* Curve for Sand Layer . . . 30
2.2.2.2. *t-z* Curve for Clay Layer . . . 31
2.2.3. *Q-z* Curves . . . 32
2.3. FEM Updating . . . 35
3. PERFORMANCE ASSESSMENT . . . 41
3.1. Pushover Analysis . . . 41
3.2. Demand-Capacity Spectrum Approach . . . 47
3.3. Seismic Fragility Analysis . . . 52
4. RESONANCE PHENOMENON . . . 58

5. CAPACITY CHECKS 61
5.1. Specification for Structural Steel Buildings (AISC, 2016) 61
5.2. Guide to Stability Design Criteria for Metal Structures (Ziemian) . . . 63
6. CONCLUSION 66
REFERENCES 71

LIST OF FIGURES

Figure 2.1. The Wind Turbine Investigated in the Study. 18

Figure 2.2. Pile Cap of the Wind Turbine. 21

Figure 2.3. Pile Plan. 21

Figure 2.4. Initial Modulus of Subgrade Reaction [45]. 24

Figure 2.5. Graph for C_1, C_2, and C_3 Coefficients [45]. 26

Figure 2.6. Lateral Load-Displacement (p-y) Relationship of Sand Layer. . . . 27

Figure 2.7. t-z Curves for Sand and Clay Layers [45]. 29

Figure 2.8. Simplified Approach Used in the Calculation of Overburden Pressure. 31

Figure 2.9. Finite Element Model of the Wind Turbine including Foundation and Soil Springs. 34

Figure 2.10. Error Function for Fore-Aft Direction Case. 37

Figure 2.11. Error Function for Side-to-Side Direction Case. 37

Figure 2.12. Mode Shape Comparison for Fore-Aft Direction Case. 39

Figure 2.13. Mode Shape Comparison for Side-to-Side Direction Case. 40

Figure 3.1. Stress-Strain Diagram of Structural Steel. 41

Figure 3.2. Nonlinear Model Developed in ANSYS. 43

Figure 3.3. Pushover Curves. 44

Figure 3.4. Stress Distributions at Different Steps of Pushover Analysis. . . . 45

Figure 3.5. Initial Imperfection Defined in the Model. 46

Figure 3.6. Pushover Curves for Different Imperfection Cases. 47

Figure 3.7. Modal Capacity Curve. 49

Figure 3.8. Design Spectrum. 50

Figure 3.9. Modal Displacement Demand Curve. 51

Figure 3.10. Comparison of Demand and Capacity Curves. 51

Figure 3.11. Comparison of Design Spectrum with Geometric Mean Spectrum. 54

Figure 3.12. Comparison of Design Spectrum with Response Spectra of Earthquakes. 54

Figure 3.13. Visual Representation of Wind Field [51]. 55

Figure 3.14. Rotor Thrust Time Histories obtained from FAST. 56

Figure 3.15. Fragility Curves. 57

Figure 4.1. Resonance Peaks [55]. 59

Figure 4.2. Campbell Diagram. 59

Figure 4.3. Comparison of Acceleration and Rotor Speed Time Histories. . . . 60

Figure 5.1. Experimental Data for Moment Capacity [58]. 63

Figure 5.2. Bending Moment Demand under Darfield Earthquake and Analytical Capacities. 65

Figure 5.3. Bending Moment Demand under Imperial Valley Earthquake and Analytical Capacities. 65

LIST OF TABLES

Table 2.1. Properties of Steel Tower Parts 19

Table 2.2. Wall Thickness Through Height 19

Table 2.3. Properties of the Wind Turbine 20

Table 2.4. Soil Properties 22

Table 2.5. C_1, C_2, and C_3 Coefficients 26

Table 2.6. Ultimate Bearing Capacities for Shallow and Deep Depths 26

Table 2.7. p-y Relationship for Clay Layer 28

Table 2.8. t-z Curve Coordinates for Sand Layer 30

Table 2.9. t-z Curve Coordinates for Clay Layer 31

Table 2.10. Q-z Curve Coordinates 32

Table 2.11. Soil Spring Constants 33

Table 2.12. Weighting Coefficients Used in Error Function 36

Table 2.13. Natural Frequency Comparison 38

Table 3.1. Mass and Stiffness Constants 43

Table 3.2. Effective Modal Mass and Modal Participation Factors for the First Mode 48

LIST OF SYMBOLS

$3f$	Blade Passage Frequency
a_0	Mass Coefficient
a_1	Stiffness Coefficient
A	Coefficient to Account for Cyclic and Static Loading
A_1	Spectral Acceleration for Mode 1
A_p	Gross End Area of Pile
c	Undrained Shear Strength
C_1, C_2, C_3	Coefficients
D	Pile Diameter
E	Young's Modulus
Er	Error Function
f_i^*	Identified Natural Frequency for Mode i
f_i^*	Obtained Natural Frequency from the FEM for Mode i
$F(.)$	Fragility Curve for a Specific State of Damage
F_y	Critical Buckling Stress
F_y	Yield Stress
g	Gravitational Acceleration
H	Depth
h_i	Weighting Coefficient for Mode Shapes of Mode i
IM	Intensity Measure
J	Dimensionless Constant
k	Initial Modulus of Subgrade Reaction
k_i	Weighting Coefficient for Natural Frequency of Mode i
K	Lateral Earth Pressure Coefficient
L	Maximum Likelihood Function
med	Median
M_n	Nominal Moment Capacity
M_p	Plastic Moment Capacity

M_u	Ultimate Moment Capacity
M_{x1}	Effective Modal Mass of First Mode
n	Number of Blades
N	Number of Ground Motions
P	Lateral Soil Resistance
P_0	Effective Overburden Pressure
p_u	Ultimate Bearing Capacity
p_{ud}	Ultimate Bearing Capacity for Deep Depth
p_{us}	Ultimate Bearing Capacity for Shallow Depth
q	Unit End Bearing Capacity
Q	Mobilized End Bearing Capacity
Q_p	Total End Bearing
s	Log Standard Deviation
S	Elastic Section Modulus
S_a	Spectral Acceleration
S_d	Spectral Displacement
t	Mobilized Soil Pile Adhesion
t_{max}	Maximum Soil Pile Adhesion
t_w	Design Wall Thickness
T_1	Natural Period of the First Mode
$U_{top,1}$	Displacement Demand at the Top of the Tower
V_1	Base Shear Demand
w_1	Natural Frequency of the First Mode
w_n	Natural Frequency of Mode n
x_i	Damage Case
X	Depth Below Soil Surface
X_R	Depth Below Soil Surface to Bottom of Reduced Resistance Zone
y	Lateral Displacement
y_c	Lateral Deflection Capacity
z	Local Pile Deflection

Z	Plastic Section Modulus
γ	Effective Soil Weight
Γ_1	Participation Factor for the First Mode
δ	Internal Angle between Soil and Pile Wall
ϵ_c	Constant for Lateral Deflection Capacity
ζ_n	Specified Damping Ratio of Mode n
λ_p	Limiting Width-to-Thickness Ratio for Compact Sections
λ_r	Limiting Width-to-Thickness Ratio for Noncompact Sections
σ_y	Yield Stress
ϕ	Internal Friction Angle
$\phi[.]$	Standardized Normal Distribution Function
$\phi_{top,1}$	First Mode Shape Amplitude at the Top of the Tower
ψ	Mode Shape Obtained from the FEM
ψ^*	Identified Mode Shape
Ω	Rotational Frequency of Blades

LIST OF ACRONYMS/ABBREVIATIONS

AISC	American Institute of Steel Construction
API	American Petroleum Institute
ASCE	American Society of Civil Engineers
CFBC	Circular Flange-Bolted Connection
FAST	Fatigue, Aerodynamics, Structures, and Turbulence
FEM	Finite Element Model
GPa	Gigapascal
GW	Gigawatt
HSS	Hollow Structural Section
Hz	Hertz
kN	Kilonewtons
kPa	Kilopascal
kW	Kilowatts
m	Meters
MAC	Modal Assurance Criterion
mm	Millimeters
MPa	Megapascal
MW	Megawatts
NREL	National Renewable Energy Laboratory
PGA	Peak Ground Acceleration
PGV	Peak Ground Velocity
rpm	Revolutions per Minute
SA	Spectral Acceleration
SI	Spectrum Intensity
SV	Spectral Velocity
SIWEC	Simulation of Wind Energy Converters
SRSS	Square Root of Sum of Squares
TurbSim	Turbulence Simulator

TWEA	Turkish Wind Energy Association

1. INTRODUCTION

1.1. Overview

Energy has an important role in today's world and the importance of it increases day by day. As the demand for energy has increased and global warming has become an important problem for the world, investments in renewable energy sources and the share of the usage of renewable energy increase all around the world.

One of the most common renewable energy sources is wind energy. The usage of wind energy increases rapidly since it is continuous, serviceable, and environmentally friendly. Governments make huge investments in wind turbines that have slender structures with concentrated masses on top of them, therefore their structural health monitoring must be performed carefully and their dynamic characteristics must be understood very well.

In parallel with the world, investments in wind energy and the number of wind turbines have been increasing tremendously in Turkey for the last 20 years. In this scope, a 900-kW wind turbine is constructed on the Kilyos-Sarıtepe Campus of Boğaziçi University which has a significant wind energy potential. This campus is the first and only green campus in Turkey as all the electric energy need of the campus is provided by this wind turbine. Real-time structural health monitoring of this wind turbine is performed continuously via accelerometers and strain gauges placed on it to track possible damages under wind and seismic loadings.

Structural health monitoring of wind turbines not only gives a chance to track possible damages but also provides a reference point for the finite element modeling of them. The finite element model development of wind turbines is necessary to simulate the structural behavior of them under possible wind and earthquake loadings.

1.2. Objective

This study aims to assess the structural performance of a 900 kW wind turbine located in the Kilyos-Sarıtepe Campus of the Boğaziçi University under expected wind and earthquake excitations on the site. Turkey is in a seismic zone therefore performance assessment of this wind turbine should have been done attentively.

The wind turbine has a slender structure with 54 m hub height. Nacelle and rotor parts lead to eccentric loading on top of the wind turbine which influences the structural behavior. The wind turbine foundation includes 26 identical piles in circular form with 2 layers. Soil deposit of the wind turbine site is composed of sand and clay layers. Investigation of the soil flexibility effects is an important part of this study.

In order to develop a successful investigation of the wind turbine performance, a detailed finite element model is developed in SAP2000 according to the identified dynamic properties. Dynamic parameters obtained from the initial FEM slightly differ from identified values because of uncertainty in steel Young's modulus and soil stiffness. For this reason, FEM updating is performed to minimize the difference between real structure and the finite element model.

Also, a nonlinear finite element model of the wind turbine including soil flexibility is developed in ANSYS software to investigate the buckling behavior of the tubular steel tower. In the nonlinear model of the wind turbine, steel Young's modulus and soil stiffness parameters found from the FEM updating process are used to represent the real structure with the highest level of accuracy.

The wind turbine is close to the North Anatolian Fault therefore fragility curves are developed to assess the structural performance using 11 earthquakes that have similar characteristics with the design spectrum of the site . Also, wind loads for different mean wind speeds are considered to investigate the wind load effect on the structural performance of the wind turbine.

1.3. Literature Review

In the literature, lots of studies exist concerning the design concepts, seismic resistance, and the investigation of the soil flexibility effects on the structural behavior of both onshore and offshore wind turbines. In these studies, seismic response analyses of wind turbines are investigated through either experimentally or with the help of finite element models. There are two concepts for the soil flexibility effects which are shallow and piled foundation concepts. Studies for each of these concepts are reviewed for this thesis. The subject of this study is to investigate the structural performance and monitor the dynamic properties of the wind turbine under earthquake and wind loads therefore studies related to damage identification and collapse risk assessment are reviewed throughout this study.

Asareh *et al.* [1] implemented a seismic module to the FAST code and developed a computational platform that provides combined simulations of seismic and wind load actions. From the motion handling approaches used in the platform, the baseline correction method removes residual displacement or velocity while the target response spectral matching method modifies input motion to produce the desired response spectrum. The effect of the aerodynamic damping on the structural response is investigated. Coupled simulations are compared with linear load combinations of seismic and operational loads. It is concluded that linear combination results in overestimation.

Asareh and Prowell [2] compared the simulation results of coupled-model with the results of several combining approaches of individual analyses. They conducted the direct-coupled simulations in FAST software for three loading scenarios; idling, operating and emergency shutdown. Simulations in FAST considering only operational loads and simulations in OpenSees considering only seismic action are conducted. Linear, SRSS, and ASCE recommendations are used for load combinations and results of these combinations are compared with coupled simulation results. Comparisons show that SRSS and ASCE combinations give similar results with coupled simulation. However, using the linear combination overestimates the structural responses.

Valamanesh and Myers [3] developed a closed-form solution based on blade element momentum theory for aerodynamic damping of horizontal axis wind turbines. Aerodynamic damping values in both directions are predicted analytically with the developed formulation. Wind loads are found by numerical methods. Damping predictions are compared with the results found from FAST software for a 1.5 MW wind turbine. Results show that a good correlation is seen. Also, the effects of simplification assumptions on structural aerodynamic damping are discussed. The dynamic model of the wind turbine is analyzed under 7 ground motions and the effect of aerodynamic damping on the structural response is investigated.

Eads *et al.* [4] discussed various parameters affecting fragility curve computation and presented an efficient method to compute collapse fragility curves. Fragility curves are combined with seismic hazard curves to carry out a collapse risk assessment. They defined the deaggregation of collapse risk to identify the contribution of ground motion intensities to total collapse risk. It is indicated that ground motion intensities in the first half of the fragility curve dominate the mean rate of collapse per year. The uncertainties in obtaining fragility curves and the mean rate of collapse per year are discussed. It is indicated that using a low number of ground motions leads to large errors. A new method is proposed for the assessment of collapse risk. It is concluded that the new method reduces computational effort and minimizes uncertainties.

Lavassas *et al.* [5] presented the basic properties of the analysis and design of a 1 MW wind turbine tower prototype. They developed a simplified and a complete finite element model of the wind turbine. Wind load and fatigue phenomena are discussed. Spectral response analysis is carried out. The design of the wind turbine prototype is completed applying the trial-and-error approach. Also, detailed finite element models of flange connections are presented. It is stated that the simplified model is enough for basic response and dynamic property calculations but it is not sufficient for the ultimate limit state since local stress concentrations are neglected. It is indicated that extreme wind load is critical for the wind turbine prototype. However, it is also stated that seismic design may be the critical one for wind turbines in seismic regions.

Yang *et al.* [6] proposed a new method for damage detection. They stated that damage is a local phenomenon and finite element modeling of a complex structure involves many degrees of freedom. A large number of degrees of freedom lead to heavy computational efforts and a large number of sensor requirements. Therefore, a damage detection method related to reduced-order finite element formulation based on static condensation is proposed to identify the loosening of bolted connections. A shake table test of a six-story structure is performed to investigate the validity of the proposed method. Results show that the proposed method is capable of detecting damages due to the loosening of bolts in the joints.

Kiyomiya *et al.* [7] investigated the combined effects of wind and earthquake loads from a probabilistic point of view. The Weibull distribution function is used for each loading types and joint probability density is found by multiplying two probability densities. It is observed that the occurrence probability of two extreme loadings at the same time is very small. The model of the wind turbine is developed, and dynamic analysis is performed. It is seen that both top displacement and bending moments at the base are proportional to input motions. Also, it is indicated that wind turbine towers have high seismic capacity when they are designed due to strong wind loads.

Staino and Basu [8] investigated modeling and controlling the vibrational responses that occur due to fluctuations in the rotor speed of wind turbines. They developed a multi-modal horizontal axis wind turbine model formulation with variational rotor speed. Variation in the rotor speed is considered in the stiffness matrix of the model. It is concluded that variations in the rotor speed cause severe edgewise vibrations. Vibration controllers are defined which are placed on blades to eliminate edgewise vibration demands. It is seen that the proposed vibration controllers successfully eliminate large vibration demands of blades.

Blachowski and Gutkowski [9] examined the behavior of circular flange-bolted connection (CFBC) of a telecommunication tower. They carry out a detailed FEM analysis on ABAQUS software. Static condensation is used to reduce the number of

degrees of freedom. FEM analyses are carried out for different pre-stressing loads and flange thicknesses. It is seen that CFBC rigidity is strongly related to these two parameters. Also, the influence of these parameters on the prying effect is investigated and it is observed that they have an important influence on the prying effect. Finally, analyses of structures with healthy and damaged connections are compared. A significant difference is not seen between two cases in terms of deformations of towers.

Prowell *et al.* [10] conducted FAST simulations of a wind turbine under seismic actions for idling, operating and shutdown cases and compared the results. They used 22 earthquake records which are scaled to reduce variability in PGV. These normalized earthquake records are multiplied with 1.3. Finally, tower moment demand values at specified elevations are presented for each operational state and the influence of the operational state on the seismic response of the wind turbine is discussed.

Prowell *et al.* [11] performed a full-scale shake table test of a 23-m wind turbine to investigate the characteristics of the seismic response. The input motion is filtered to eliminate high-frequency noise. Modal properties of the wind turbine are obtained from experimental results. Two finite element models are developed, their natural frequencies are compared with the experimental results and a good correlation is observed. It is also indicated that two models give similar results except for third bending mode frequency which differs slightly due to eccentric loading in model two. The effect of damping on structural response is investigated. Response spectrum analysis results of wind turbines are compared with FEM results and good agreement is seen.

Cao and Bell [12] performed experimental tests of four circular flanges under static tension force. Bolt forces and tension forces are measured to obtain prying forces that have an important effect on joint behavior. The curves representing relationships between bolt forces and tension forces for different preloads are presented. The stiffnesses of joints are compared according to the relationships between tension forces and joint displacements. Finally, stress measurements are compared with previously developed finite element model and a good correlation is seen.

Prowell *et al.* [13] discussed recent additions to the FAST software which allows users to consider seismic load in addition to operational loads. For this purpose, two numerical models of a wind turbine are developed both on OpenSees and FAST. Dynamic simulations for three earthquake records are conducted for the idling state of the turbine since OpenSees cannot consider operational loads. Acceleration time histories and moment demands are compared and good agreement is obtained.

Sim *et al.* [14] investigated the flexural strength and failure mode of a wind turbine tower through full-scale displacement controlled static test. Results show that strength degradation occurs due to local buckling, however, the tower shows a good post-buckling ductility. A parametric analysis is performed to investigate the effects of boundary conditions and wall local dent. Boundary conditions have a significant effect on the ultimate strength and failure mode. On the other hand, the existence of local dent has an important influence on location and type of local buckling. Also, very good correlation is obtained between experimental results and FEM results.

Quilligan *et al.* [15] investigated relative performances of concrete and steel tower solutions to a numerical model for various tower heights and wind speeds. Centrifugal stiffening is taken into account. The drag force component of wind loading is obtained analytically as time series. The frequency content of displacement time history is observed to identify the important frequencies in which the tower vibrates. It is seen that the first peak occurs at the natural frequency of the tower, on the other hand, the second peak occurs at the rotational speed of blades. It is observed that displacement responses are higher for steel towers. It is also indicated that responses increase as tower height increases. Finally, hub displacement-based fragility analysis is developed. The fragility hazard parameter is chosen as the hub height wind speed.

Prowell *et al.* [16] presented an overview of a full-scale shake table test of a wind turbine. They provided the physical properties of the wind turbine and defined the experimental program. Responses of the turbine for different levels of input accelerations are provided. Also, damping values according to log decrement and half-power

band approaches are obtained for different levels of an earthquake. Results show that two approaches give similar damping values.

Drenick *et al.* [17] examined both the revenues and costs of three potential wind farms. Energy generations are determined according to multi-year time history analyses based on local wind conditions and potential revenue of each site. The costs of wind farms on each site are determined according to three parameters which are water depth, distance to shore, and distance from the port. Results show that cost of the same wind farm may vary significantly based on the location of the site.

Pollino and Huckelbridge [18] discussed fatigue demands of a 100 kW wind turbine tower according to the Palmgren-Miner principle using monitored structural demands for approximately 1 year period. The rain-flow counting method is used to calculate fatigue measurements. Fatigue capacities of different parts of the wind turbine tower are compared with the fatigue demands to estimate the remaining fatigue life of the structure. Cycles of two of these tower sections don't exceed threshold stresses which means they theoretically don't experience fatigue damage. The other two parts experience fatigue damages, however, the minimum fatigue life is calculated as 280 years.

Seidel and Schaumann [19] discussed experimental and numerical investigations of bolted connections of steel tubular wind turbine towers. The experimental part of the study is carried out to observe the relationship between bolt stresses and external loads. For this purpose, both laboratory tests of flange segments and tests in operating wind turbines are performed. Then, finite element models of one flange segment and the total flange are set up. Three simplified calculation models are used to assess flanges. It is concluded that fatigue assessment can be done with the segment model rather than the total flange model since both models give very similar results.

Prowell *et al.* [20] investigated a combination of conventional instruments and point tracking videogrammetry for capturing the global response of a wind turbine. In this new method traditional strain, displacement, and acceleration instruments are

used for the responses of the wind turbine tower and videogrammetry is used for the responses of blades. Absolute displacement values captured by conventional instruments and videogrammetry are compared and very good agreement is observed.

Nuta *et al.* [21] outlined a general methodology that uses the finite element method to investigate the probability of reaching damage states. They presented a general methodology since there are various designs for wind turbines. A finite element model is developed for an experimental specimen in the literature. The model is subjected to the same ground motion used in the shake table test and reasonable agreement is obtained. Pushover and time history analyses are performed for a 1.65 MW wind turbine and buckling failure is seen in both analyses. The incremental dynamic analysis is performed and fragility curves are developed to assess the structural performance of the wind turbine.

Prowell *et al.* [22] investigated the soil-structure interaction (SSI) effect on the seismic response of a wind turbine. The FEM of the wind turbine with a soil medium and foundation is developed. Soil is modeled with huge dimensions to eliminate boundary effects. Modal analyses are made for stiff, medium-stiff, and soft soil cases. Three models with different soil conditions are subjected to an earthquake to assess the SSI effect on structural responses. Simulations show that maximum bending moment and shear demands are observed in the model with medium-stiff soil conditions.

Ishihara and Sarwar [23] investigated seismic response characteristics of wind turbines and developed a design formula based on the response spectrum method to predict seismic loads. Eigenvector and dynamic response analyses are performed for two wind turbine towers to investigate the contribution of higher modes to seismic responses. Results show that higher mode contribution is negligible for the 400 kW turbine, however, it is significant for the 2 MW turbine. Also, the suitability of the proposed design spectrum is examined. It is seen that it gives reasonable results for low-period turbines, however, it overestimates the seismic load for high-period turbines. They conclude that period dependent safety should be used to estimate seismic loads.

Mensah *et al.* [24] carried out a probabilistic study to investigate resistance and load factors for wind turbines in seismic zones. A utility-scale 5 MW wind turbine tower model is subjected to various combinations of wind and seismic loads. Structural responses to these load combinations are simulated using the FAST code. Reliability analysis parameters are explained. Parameters of random variables that are used for tower resistance, and operational and seismic loads are provided. Finally, an equation with partial load factors for operational and earthquake loads, and a resistance factor is presented. Reliability analysis and probability models are developed.

Guo *et al.* [25] performed a complete pushover analysis of a wind turbine. They developed the finite element model of the wind turbine on ABAQUS. The influence of considering dead load is investigated. The pushover analysis shows that once the local buckling occurs, further loading causes a sudden decrease in bearing capacity. Stress distribution on the section where local buckling occurs is investigated. Also, initial geometric imperfections are considered in the analysis. Moment capacities of each section are calculated according to the 2005 AISC Specification and demand capacity ratios are calculated. Results show that the highest demand capacity ratio is obtained at the section where local buckling occurs in pushover analysis.

Stamatopoulos [26] investigated the sufficiency of the Greek Aseismic Code. For this purpose, the seismic behavior of a wind turbine is investigated with response spectrum analysis. A dynamic analysis is performed according to local response spectra for two different earthquakes. Then, a nonlinear time-history analysis is conducted. Results show that bending moment and base shear capacities calculated according to the Greek Code are much lower than demand values obtained from analyses although the design spectrum is increased by 25 percent. Accordingly, it is concluded that Greek Aseismic Code requirements are insufficient, and they should be reconsidered.

Díaz and Suárez [27] developed an analytical model for the seismic analysis of an operating wind turbine that considers the flexibility of the tower and blades. Dynamic properties of a wind turbine are obtained according to developed methodology and

seismic response analyses under various earthquake motions are performed. Analysis results show that lateral displacements of the wind turbine are larger than frontal displacements since the aerodynamic damping is negligible in lateral direction. Also, it is indicated that the tower is excited mostly in the first two modes. Stress analysis shows that all stress values remain below allowable stress limit and no structural damage occurs. It is also observed that the extreme wind is the governing load case.

Hongwang [28] investigated SSI and P-delta effects on responses of wind turbines under horizontal and vertical earthquake actions. The FEM of the wind turbine tower including soil springs is presented. Finite element models of 1.65 MW and 3 MW wind turbines are developed and time-history analyses are performed. Analysis results show that SSI has a significant influence on dynamic properties; horizontal acceleration, base moment, and base shear demands. However, SSI has no influence on vertical acceleration and axial load demands. Additionally, it is indicated that earthquake contribution to the base shear and base moment demands is remarkable.

He and Li [29] proposed a numerical method that includes an iterative process which modifies earthquake records to make their response spectra be consistent with the target spectrum. They used the Preumont method. In the modification process, the Fourier transform of time histories are modified and inverse Fourier transform is computed to find modified time histories. Seismic response analyses of two different finite element models with and without considering the SSI effect are performed. Results show that SSI has an important influence on seismic response characteristics.

Kafali and Grigoriu [30] presented the lack of correlations between PGA and spectral displacement, and between pseudo-spectral acceleration and spectral displacement. They proposed alternative intensities for fragility analysis. A good correlation is seen between white noise intensity and spectral displacement. Source-to-site and moment magnitude variables are proposed as fragility intensities and a new method is developed for calculating the system's fragility surface. Fragility analysis of the system is carried out by obtaining fragility surfaces for different limit states.

Zhao and Maisser [31] developed a multi-body model that considers the SSI effect and investigated its dynamic responses under seismic action. They identify spring constant formulas for each degree of freedom. The wind turbine tower is modeled with discretized joint beam elements. The equation of motion of the system is derived from the Lagrangian approach. Wind load calculations are explained. For wind load calculations, the blade element theory is used. Simulations under wind and seismic loadings are performed for models with and without SSI effects. It is concluded that SSI has an important effect on the dynamic properties of structures.

Kjørlaug *et al.* [32] performed a dynamic response analysis of a wind turbine. A wind turbine model which was studied before is developed in SAP2000 and the model is verified as a good agreement is seen for both dynamic properties and dynamic responses. Then, a model of 5 MW wind turbine is developed including the soil and the mono-pile to account for SSI. This model is excited by scaled versions of the Nahanni earthquake. Wind load is applied as a static load. It is indicated that the vertical component of the earthquake can cause high acceleration demands on the top parts of the turbine. It is also concluded that the SSI has an important influence on responses.

Prowell *et al.* [33] presented experimental shake table test results of a full-scale wind turbine. They developed a finite element of the wind turbine using beam-column elements which is calibrated according to the experimental results. The model is subjected to 5 different seismic events and only one of these earthquakes makes moment response of the wind turbine reach the predefined threshold. Also, the differences in structural demands caused by uni-axial and bi-directional seismic loadings are investigated. It is concluded that moment demand increase due to weak component is very low and falls below the requirements of the code.

Prowell *et al.* [34] performed shake table tests of a 65-kW wind turbine to investigate dynamic properties and structural demands of the wind turbine under earthquake and operational loads. Each test is performed for parked and operational states. Tests are performed in both fore-aft and side-to-side directions. The influence of the oper-

ational effects on the seismic response is discussed. Numerical simulations are carried out both with OpenSees and modified version of FAST software. The OpenSees model provided good results for the parked condition. When FAST simulation results are compared with experimental results good agreement is seen. When FAST and OpenSees results are compared, lower errors are seen in the FAST model for operating conditions.

Prowell *et al.* [35] developed a finite element model of the wind turbine according to shake table tests. A good correlation is obtained between the FEM and the full-scale test results. The FEM is analyzed under various earthquake records. The dynamic properties of the full-scale wind turbine are determined. Stiffness degradation in the wind turbine is examined. Possible sources of overall stiffness degradation are stated as, stiffness degradation in base connection and loosening of bolts. Simulations of earthquake actions show that structural response demands in different directions differ slightly. Also, it is indicated that higher modes of the wind turbine become important for excitations with high-frequency content.

Bazeos *et al.* [36] investigated seismic behavior and load-bearing capacity of a 450-kW wind turbine tower. Determination of load combination that creates local buckling, the influence of door opening, and the influence of SSI effects are investigated. They carried out 5 different analyses. In static analysis, pseudo-aerodynamic and dead loads are subjected to the model, and stress distribution is investigated. In the elastic buckling analysis, local buckling analysis is performed under axial, flexural, and torsional loads. In the seismic analysis, the results of the finite element model and the simplified model are investigated. In the fixed-base analysis, the finite element model and the simplified model are compared. In the elastic subgrade analysis, soil springs are introduced to models and dynamic properties are compared with fixed-base models.

Patil *et al.* [37] performed a seismic performance assessment of a wind turbine. A detailed FEM is developed in ANSYS in which bolted connections and the door are modeled. Aerodynamic damping and operational loads are ignored. Seismic fragility analyses are performed. Limit states used in fragility analyses are global buckling,

first yielding occurrence, overturning of foundation, and permanent deformation of the steel tower. After fragility curves are obtained, it is seen that the tower is the most vulnerable to overturning limit state. Other limit states can be ordered as yielding, permanent deformation and buckling of steel tower from most vulnerable to the least.

Robertson *et al.* [38] investigated test data from the experiments of a floating wind system performed by a group of universities to understand the complex dynamic behavior of floating wind systems. Experimental data are used for the validation of the FAST. Tests of three different wind system models are conducted throughout the program. Models are tested under various wind and wave conditions.

Haenler *et al.* [39] developed a simulation code for wind turbines used in load calculations and determination of dynamic properties. In this code, wind turbine components are modeled by a variable number of modes to enable adjusting the degrees of freedom. The SSI effect is included in the code. A program that creates three-dimensional earthquake time-series is created. A seismic analysis of the wind turbine is carried out. It is seen that amplitude increase in higher modes due to earthquake action is stronger than the first mode of vibration. Also, it is shown that most of the total vibration energy is contained in the first two modes.

Drenick *et al.* [40] investigated the influence of wind data resolution sets on final energy output and they predicted revenue from offshore wind farms. Four different data sets are analyzed. For two of these sets, time history analyses are made. For others, probabilistic approaches are used. Expected energy and revenue is presented for each data set at each site. Research shows that generated energy and revenue values obtained by the probabilistic approach may differ from time history analysis. Energy generation results correlate for each data set but predicted revenues differ significantly.

Kjørlaug and Kaynia [41] investigated the structural dynamic response of a wind turbine under vertical components of earthquakes. A model for a 5 MW wind turbine is developed which considers SSI effects. Earthquake analysis of the wind turbine is

carried out by the spring model, coupled model, and deep soil model. In the spring model, soil springs are assigned at the base of the model. Analysis results in large amplification of the vertical response. In the coupled model, both the structure and the foundation including the soil are modeled. Results correlate with the spring model. In deep soil model, a wind turbine in deep soil medium is considered to capture true vertical amplification. The results of this model show lower magnitudes in response since soil amplification between bedrock and ground surface is eliminated.

Bozorgnia *et al.* [42] presented vertical response analyses of twelve instrumented structures. Distance-dependent vertical and horizontal response spectra are generated. It is indicated that vertical to horizontal response ratio is source-to-site distance and period dependent. Also, obtaining vertical spectra from horizontal response spectra with an approximate procedure is discussed. Analysis results of all structures are presented. Plots of transfer functions, coherence functions, phase angles, and cross-spectra are presented and the results are discussed.

Hu *et al.* [43] investigated the resonance phenomenon of a wind turbine. Analytical and experimental Campbell diagrams are presented. It is notified that the fundamental frequency of the tower is in the 3f region which leads to resonance. When the rotor speed approaches the resonance frequency, the vibration amplitude of the tower increases significantly. Sommerfeld effect is explained. It is concluded that the Sommerfeld effect may make wind turbines get stuck in resonance. Accordingly, the necessity of vibration control devices that minimize excessive vibrations is stated.

Katsanos *et al.* [44] presented a detailed review of current methods, studies about modeling techniques, and evaluations of seismic analysis results. They state that seismic action for wind turbines is essential. They indicate that wind turbines are considered as 'self-isolated' against earthquakes since they have large natural periods, however, they discuss that this notion may be misleading and risky. Numerical studies that rely on deterministic and probabilistic approaches to investigate the structural behavior of wind turbines are examined. Studies considering SSI effects are reviewed.

1.4. Scope

In chapter one, an overview of the wind energy and the usage of wind turbines is presented, the goal of this study is indicated and a comprehensive literature review concerning various concepts of wind turbines is made.

In chapter two, all details of the steel tower, concrete foundation, and the soil deposit of the wind turbine are given and the development of the complete finite element model of the structure is demonstrated. The finite element model is developed in SAP2000 software. The soil is represented by soil springs attached to piles of the foundation. Calculations of soil spring stiffnesses are presented in detail and the complete finite element model of the wind turbine is given. Then, FEM updating is performed. In this process, identified natural frequencies and mode shapes obtained in previous works are taken as reference. In the updating process, only the first three modes are used. Steel Young's modulus and soil spring stiffness coefficients are taken as updating parameters. An error function is identified and the error values for each combination of updating parameters are recorded. Finally, an error surface is created according to calculated error values and the combination of parameters giving minimum error value is taken for the final version of the finite element model.

In chapter three, the performance assessment of the wind turbine is carried out. For this purpose, nonlinear pushover analysis is performed first. Since the finite element model developed in SAP2000 is linear, a nonlinear finite element model of the wind turbine is developed in ANSYS software with the parameters obtained from the updating process. For the foundation, a simplified method which is the global spring approach is used. For the verification, dynamic properties of the nonlinear model are compared with identified values and obtained values from SAP2000 software, and good agreement is seen. Then, the design spectrum of the wind turbine site is obtained according to the Turkish Seismic Code. Demand and capacity curves are compared to find the performance point of the structure. Then, the buckling of the steel tower is taken as the damage state and incremental dynamic analysis is performed. Fragility

curves of the wind turbine tower considering different levels of wind loading are developed. For this process, 11 earthquake records that have similar response spectra with the design spectrum of the site are used, and analyses are carried out with all three components of records.

In chapter four, the resonance phenomenon for wind turbine towers is discussed. Firstly, mass unbalance and tower dam effects which are the possible sources of resonance are explained. Then, the Campbell diagram of the wind turbine is developed and the rotor speed which is suspicious to cause resonance of the tower is determined. Finally, the real-time acceleration record of the tower in a time range that the rotor speed gets equal to the resonance rotor speed is investigated, and results are discussed.

In chapter five, the buckling capacity of the steel tower of the wind turbine considering the local buckling is calculated according to two different references. The capacities are calculated in terms of bending moment values. Then, these capacities are compared with bending moment demands obtained from different earthquake analyses to investigate the validity of analytical calculations for buckling analysis and very good agreement is observed.

2. FINITE ELEMENT MODELING

2.1. Tower, Foundation and Soil Details

In this study, a 900-kW wind tower with 55 m hub height and 44 m rotor diameter which is in the Sarıtepe Campus of Boğaziçi University is investigated. The steel tower of the wind turbine is 53.95 m which is composed of three thin-walled tubular parts. The diameter and thickness values of the steel tower vary throughout the height. The diameter of the tower is 3.3 m at the ground level and 1.33 m at the top of the tower. Wall thickness values of the steel tower vary between 12 mm and 24 mm. The wind turbine investigated in this work is given in Figure 2.1, the properties of tubular parts of the steel tower are given in Table 2.1 and wall thickness values throughout the height is given in Table 2.2.



Figure 2.1. The Wind Turbine Investigated in the Study.

Table 2.1. Properties of Steel Tower Parts.

	Bottom Elevation (m)	**Top Elevation (m)**	**Length (m)**	**Bottom Diameter (m)**	**Top Diameter (m)**
Part 1	0	17.03	17.03	3.30	2.41
Part 2	17.03	34.03	17.00	2.41	1.80
Part 3	34.03	53.95	19.92	1.80	1.33

Table 2.2. Wall Thickness Through Height.

Bottom Elevation (m)	**Top Elevation (m)**	**Thickness (mm)**
0	5.61	24
5.61	8.31	20
8.31	19.95	18
19.95	36.85	16
36.85	44.05	14
44.05	48.62	12
48.62	51.09	14
51.09	53.95	16

The material of the tower is S355 steel with Young's modulus value of 200 GPa. The total weight of the wind turbine is 860 kN where the weight of the steel tower is 534 kN and the total weight of rotor + nacelle parts is 326 kN. The center of mass of the total mass of rotor + nacelle parts is 0.85 m higher from the top of the tower and 1.52 m away from the center of the tower section in the horizontal direction which causes eccentricity. Details of the wind turbine are given in Table 2.3.

Table 2.3. Properties of the Wind Turbine.

Rated Power (kW)	900
Rotor Diameter (m)	44
Tower Height (m)	53.95
Weight of the Steel Tower (kN)	534
Total Weight of the Nacelle+Rotor (kN)	326
Horizontal Eccentricity of Nacelle+Rotor Center of Mass (m)	1.52
Vertical Eccentricity of Nacelle+Rotor Center of Mass (m)	0.85
Class of Structural Steel	S355
Young's Modulus of Steel (GPa)	200
Yield Strength of Steel (MPa)	355

The material of the foundation is C35 concrete. The foundation of the wind turbine consists of a pile cap and 26 piles. The pile cap of the wind turbine includes three parts. The top and bottom parts of the pile cap have cylindrical shapes with diameters of 5 m and 13.5 m where the middle part is an inclined section. The total depth of the pile cap is 1.6 m. Side view of the pile cap is given in Figure 2.2.

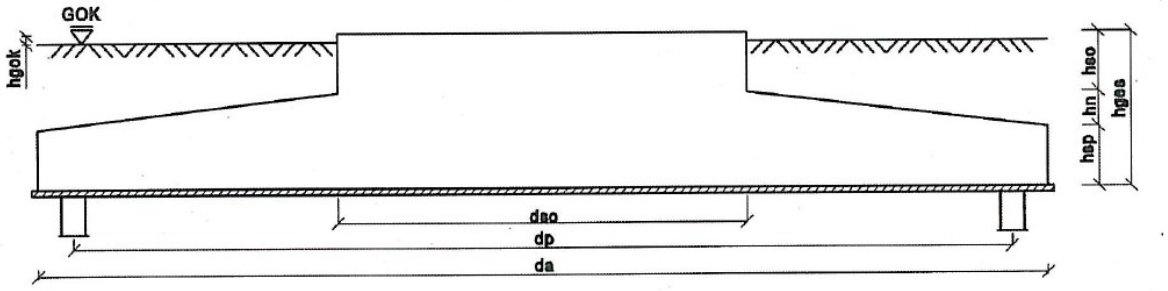

Figure 2.2. Pile Cap of the Wind Turbine.

All piles of the foundation are identical and located in circular form with two layers. The diameter of cylindrical piles is 0.4 m and the depth of the piles is 18 m. The diameter of the inner layer in the pile plan is 6.2 m while the diameter of the outer layer is 11.2 m. The inner layer includes 8 piles and the outer layer has 18 piles which have constant angles between adjacent piles. The pile plan of the foundation is given in Figure 2.3.

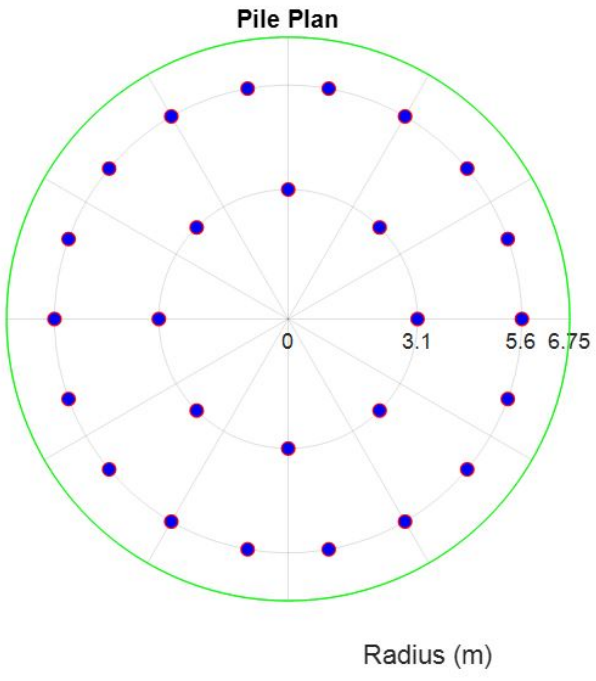

Figure 2.3. Pile Plan.

According to the geotechnical report, the soil deposit where the wind turbine is constructed has two layers which are sand and clay layers. The upper one of these layers is the sand layer with a depth of 10.5 m. Under the layer of sand, the clay layer takes place and extends to the tip of the piles. Soil properties provided in the geotechnical report are given in Table 2.4.

Table 2.4. Soil Properties.

	Sand Layer	**Clay Layer**
Depth (m)	0 - 10.5	10.5 -
Weight per Unit Volume (kg/cm2)	1.6	1.8
Cohesion (kg/cm2)	-	0.679
Internal Friction Angle, Φ (°)	22	9

2.2. Development of the Finite Element Model

The finite element model of the wind turbine considering the soil flexibility is developed in SAP2000 software. The thin-walled tubular steel tower of the structure is modeled with shell elements. Since the diameter and thickness values of the wind turbine vary along with the height, these values at 40 points along the tower height are determined. In this process, knowing the top and bottom diameters of each part of the steel tower, the inclination angles of each part of the steel tower are assumed to be constant. The circumference of the tower is divided into 40 with constant angles to make it as realistic as possible since it is not possible to create curved shell elements in SAP2000 software. Then, the steel tower of the wind turbine is developed by assigning shell elements between previously defined nodes. As the final step, these shell elements are divided into smaller sections to make their aspect ratios reasonable and to make the finite element model more realistic.

The center of mass of the total of the rotor and nacelle parts is not on the wind turbine tower, it is at a remote point which is 0.85 m higher from the top of the tower and 1.52 m away from the center of the tower section in the horizontal direction. In order to assign the mass of these parts to the remote point, two fictive elements are used which have zero masses and extremely high axial and flexural stiffness values. A body constraint is assigned to all points located at the top level of the tower to make the tower and fictive elements move together.

The pile cap and the piles are modeled with frame elements. The top and the bottom sections of the pile cap have a cylindrical shape, but the middle section has a conical shape that has varying diameter along with the height. For the diameter value of the middle section, the average of the top and bottom sections' diameter is used. As at the top of the tower, all points at the bottom of the tower, where the tower and pile cap intersect, are bonded with body constraint to make them move together. Top points of the piles are attached to the bottom of the pile cap with fictive elements that have huge axial and flexural stiffnesses. Thus, load and displacement demands on the pile cap are directly transferred to piles.

The soil deposit of the site which influences the structural behavior of the wind turbine is represented by soil springs. Soil springs are assigned to piles with 1.5 m intervals. Stiffness values of these soil springs are calculated according to the API Guideline [45]. In this guideline, three types of load-displacement relationships are defined which are p-y, t-z, and Q-z relationships. API provides different formulations for each type of load-displacement relationship for both sand and clay layers. These relationships are nonlinear but for the soil springs, initial stiffness values of each relationship are used since nonlinear springs do not exist in SAP2000 software. For checking the validity of this approach, the model is analyzed under mean wind load and displacement demands on the piles are observed. Results show that all displacement demands remain in the linear region provided in API Guideline. Explanations of these relationships are given below.

2.2.1. p-y Curves

The lateral load-displacement relationship of the soil around the lateral face of piles is represented by p-y springs.

2.2.1.1. p-y Curve for Sand Layer. The load-displacement relationship of p-y springs is found according to the following equation for sand layer.

$$p = A \times p_u \times tanh\left[\frac{k \times H}{A \times p_u} \times y\right] \tag{2.1}$$

where

p : Lateral Soil Resistance (kN/m)

A : Coefficient to account for cyclic and static loading (0.9 for cycling)

p_u : Ultimate bearing capacity (kN/m)

k : Initial modulus of subgrade reaction(kN/m^3)

H : Depth (m)

y : Lateral displacement (m)

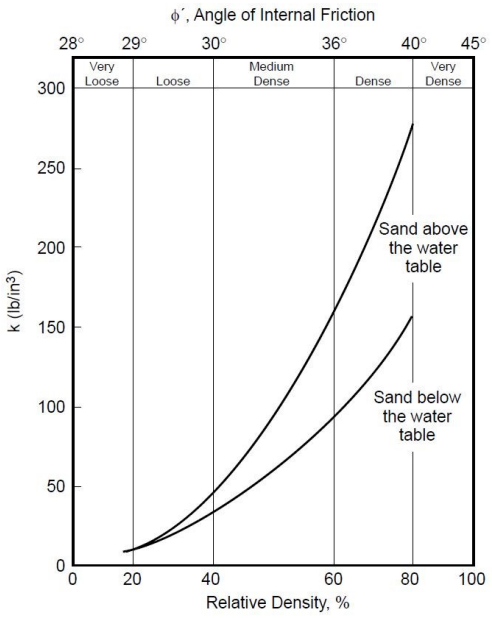

Figure 2.4. Initial Modulus of Subgrade Reaction [45].

The initial modulus of subgrade reaction is determined according to the graph provided in API Guideline which is given in Figure 2.4. Since this plot does not contain 22° of internal friction angle, it is assumed that the plot becomes constant at around 2224 kN/m^3 for values below 28° and this value is used in the calculation for the value of initial modulus of subgrade reaction.

For the ultimate bearing capacity, two different formulations are provided for shallow and deep depths and it is advised to use the smallest one from these as the ultimate bearing capacity. Ultimate bearing capacities for shallow and deep depth are provided below.

$$p_{us} = (C_1 \times H + C_2 \times D) \times \gamma \times H \tag{2.2a}$$

$$p_{ud} = C_3 \times D \times \gamma \times H \tag{2.2b}$$

where

C_1,C_2,C_3 : Coefficients

p_{us} : Ultimate bearing capacity for shallow depth(kN/m)

p_{ud} : Ultimate bearing capacity for deep depth(kN/m)

H : Depth (m)

D : Pile diameter (m)

γ : Effective soil weight(kN/m^3)

C_1, C_2, and C_3 coefficients used in the above equations are determined for the internal friction angle value of 22° according to the graph provided in API Guideline. The provided graph in API Guideline is given in Figure 2.5. C_1, C_2, and C_3 values obtained according to the provided graph are given in Table 2.5.

Ultimate bearing capacities for shallow and deep depths found by using the above formulas are given in Table 2.6.

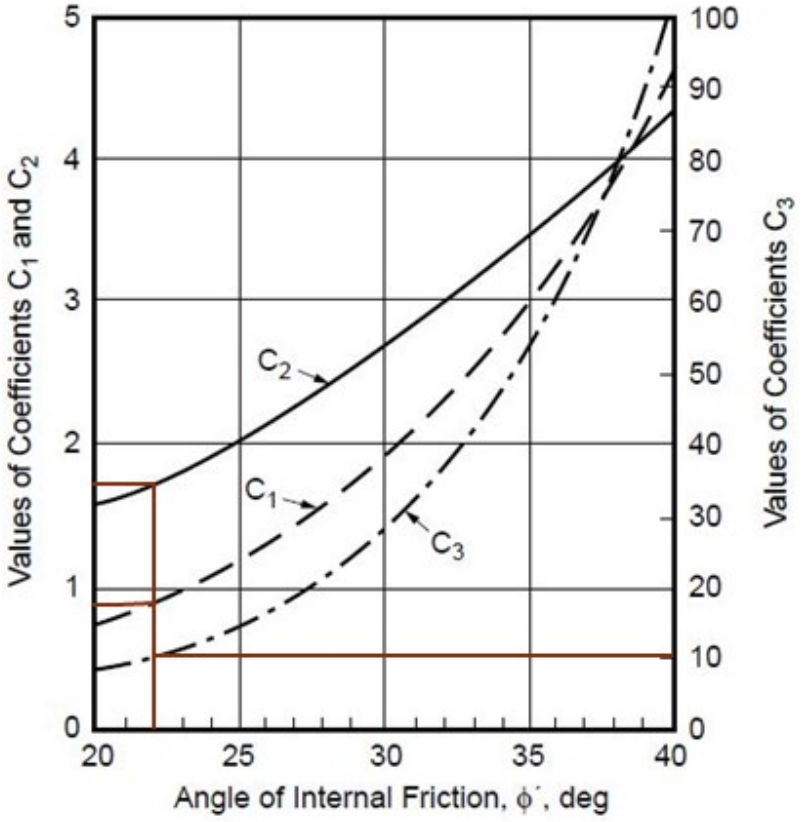

Figure 2.5. Graph for C_1, C_2, and C_3 Coefficients [45].

Table 2.5. C_1, C_2, and C_3 Coefficients.

C_1	C_2	C_3
0.9	1.7	10

Table 2.6. Ultimate Bearing Capacities for Shallow and Deep Depths.

p_{us} (kN/m)	p_{ud} (kN/m)
572.6	282.5

Giving the smaller value, the ultimate bearing capacity for deep depth is used in the formulation of the lateral load-displacement relationship of sand. *p-y* relationship of the sand layer found according to equation 2.1 is provided in Figure 2.6.

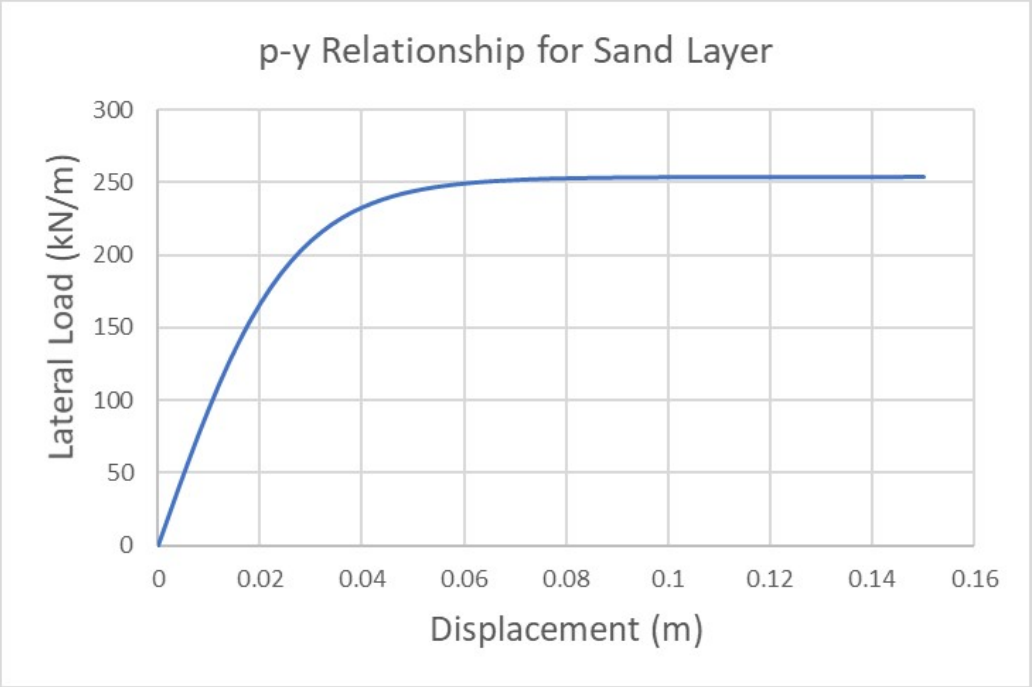

Figure 2.6. Lateral Load-Displacement (*p-y*) Relationship of Sand Layer.

Soil springs represent soil for a depth of 1.5 m therefore initial stiffness value found from the above graph is multiplied with 1.5 and the stiffness value of soil springs assigned to piles in the sand layer is calculated.

2.2.1.2. *p-y* Curve for Clay Layer. Lateral load-displacement relationship of piles in clay layers is generated according to the Table 2.7 for cycling loadings.

Table 2.7. *p-y* Relationship for Clay Layer.

$X>X_R$		$X<X_R$	
p/p_u	y/y_c	p/p_u	y/y_c
0	0	0	0
0.50	1	0.50	1
0.72	3	0.72	3
0.72	∞	0.72 X/X$_R$	15
		0.72 X/X$_R$	∞

where

X : Depth below soil surface (m)

X_R : Depth below soil surface to bottom of reduced resistance zone (m):

$$X_R = \frac{6D}{\frac{\gamma D}{c} + J} \tag{2.3}$$

D : Pile diameter (m)

γ: Effective soil weight(kN/m^3)

c : Undrained shear strength for undisturbed clay layers (kPa)

J : Dimensionless constant – ranges between 0.25 and 0.5 (taken as 0.25)

p : Actual lateral resistance (kPa)

p_u : Ultimate resistance (kPa):

$$p_u = \begin{cases} 3c + \gamma X + J\frac{cX}{D}, & \text{for X<X}_R. \\ 9c, & \text{for X}\geq\text{X}_R. \end{cases} \tag{2.4}$$

y : Actual lateral deflection (m)

y_c : 2.5 * ϵ_c * D

The constant ϵ_c ranges between 0.005-0.02 [46]. It is taken as 0.015 for this study.

Using the provided formula, X_R is found as 6.75. This shows the case where $X > X_R$ is valid in our situation since the depth of the clay layer is higher than 10.5 according to the geotechnical report. Using the above equations, ultimate resistance (p_u) is found as 599.4 kPa.

2.2.2. *t-z* Curves

The load-displacement relationship of the surrounding soil around piles under axial load is represented by *t-z* springs. This relationship concerns with the soil-pile shear transfer. Typical axial load-displacement curves and coordinates of these curves for sand and clay layers are provided in Figure 2.7.

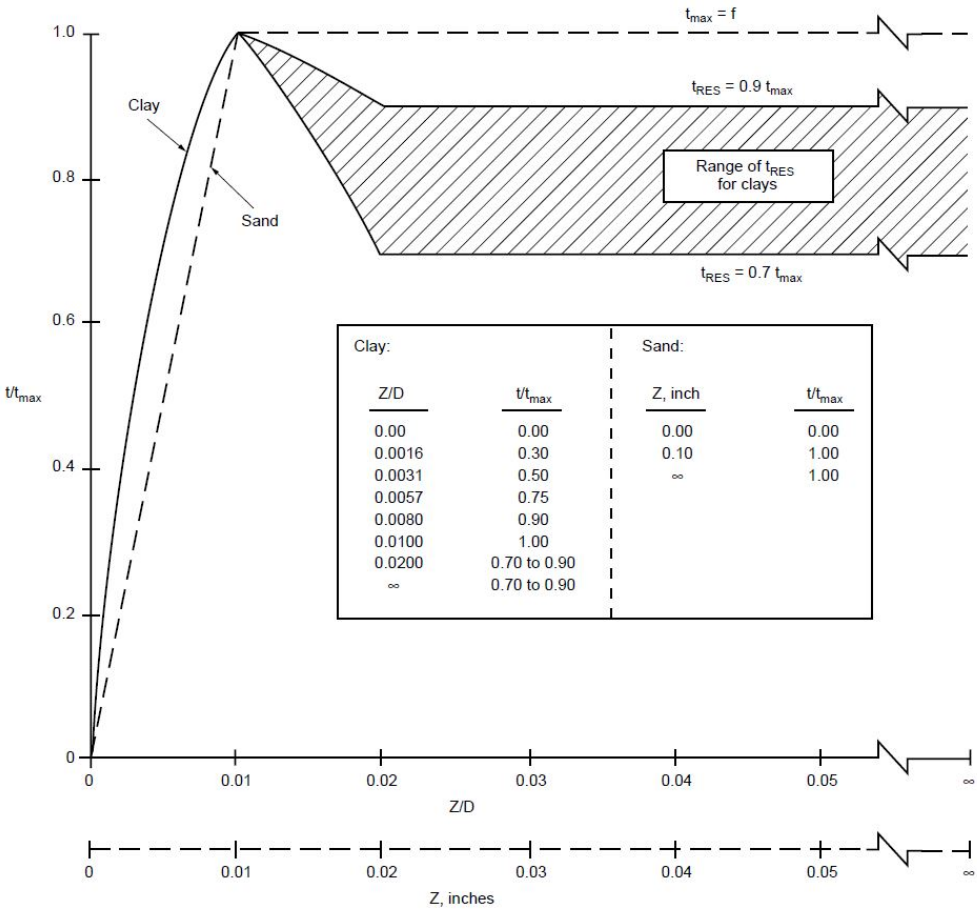

Figure 2.7. *t-z* Curves for Sand and Clay Layers [45].

2.2.2.1. t-z Curve for Sand Layer. Axial load-displacement relationship of piles in sand layer is given in Table 2.8.

Table 2.8. t-z Curve Coordinates for Sand Layer.

z (m)	t/t_{max}
0	0
0.00254	1
∞	1

where

z : Local pile deflection (m)

t : Mobilized soil pile adhesion (kPa)

t_{max}: Maximum soil pile adhesion (kPa)

$$t_{max} = K \times P_0 \times tan(\delta) \tag{2.5}$$

where

K : Lateral earth pressure coefficient (given as 0.8)

P_0 : Effective overburden pressure

δ : Internal angle between soil and pile wall

Internal angle between pile wall and soil is found according to the formula given below [47].

$$\delta = 0.75 \times \Phi \tag{2.6}$$

For the effective overburden pressure calculation, a simplified approach is used. Representation of this approach is provided in Figure 2.8.

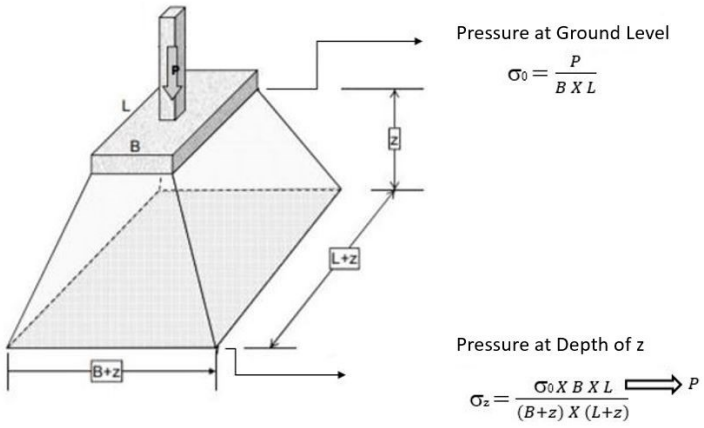

Figure 2.8. Simplified Approach Used in the Calculation of Overburden Pressure.

From the calculation, maximum soil pile adhesion is found as 23.66 kN/m^2. Using the relationship provided in Table 2.8, the slope of the t-z curve is found and the stiffness of t-z springs in the sand layer of the model is calculated by multiplying this slope with effective soil area.

2.2.2.2. t-z Curve for Clay Layer. t-z curve of piles in clay layer is developed according to Table 2.9.

Table 2.9. t-z Curve Coordinates for Clay Layer.

z/D	t/t_{max}
0	0
0.0016	0.3
0.0031	0.5
0.0057	0.75
0.008	0.9
0.01	1
0.02	0.7 to 0.9
∞	0.7 to 0.9

Maximum skin friction (t_{max}) for clay is calculated by

$$f = \alpha c \tag{2.7}$$

where

$$\alpha = \begin{cases} 0.5(c/p_0')^{-0.5}, & \text{for (c/p'}_0\text{)}\leq 1. \\ 0.5(c/p_0')^{-0.25}, & \text{for (c/p'}_0\text{)}>1. \end{cases} \tag{2.8}$$

c : Undrained shear strength (kPa)

p_0' : Effective overburden pressure (kPa)

Then, the initial slope of the t-z curve for clay is obtained and multiplied with effective soil area to calculate the stiffness of soil springs in the clay layer in the model.

2.2.3. Q-z Curves

The tip load-displacement relationship of piles is represented by the Q-z curve. The tip of piles in this project is in the clay layer. The Q-z curve for sand and clay layers is same. Coordinates of the Q-z curve provided in the API Guideline are given in Table 2.10.

Table 2.10. Q-z Curve Coordinates.

z/D	Q/Q_p
0	0
0.002	0.25
0.013	0.5
0.042	0.75
0.073	0.9
0.1	1

where

z : Axial tip deflection (m)

D : Pile diameter (m)

Q : Mobilized end bearing capacity (kN)

Qp : Total end bearing (kPa)

$$Q_p = qA_p \tag{2.9}$$

where

q : Unit end bearing capacity (kPa)

A_p : Gross end area of pile (m^2)

$$q = 9c \tag{2.10}$$

where

c : Undrained shear strength (kPa)

Using the equations above, Q-z curve is developed. Using the initial stiffness value of the Q-z curve, the stiffness value of springs assigned to the tip of piles is calculated. All soil spring constants calculated in this section are given in Table 2.11.

Table 2.11. Soil Spring Constants.

	Sand Layer	**Clay Layer**
p-y Springs (kN/m)	12123	11988
t-z Springs (kN/m)	15310	54443
Q-z Springs (kN/m)	-	23500

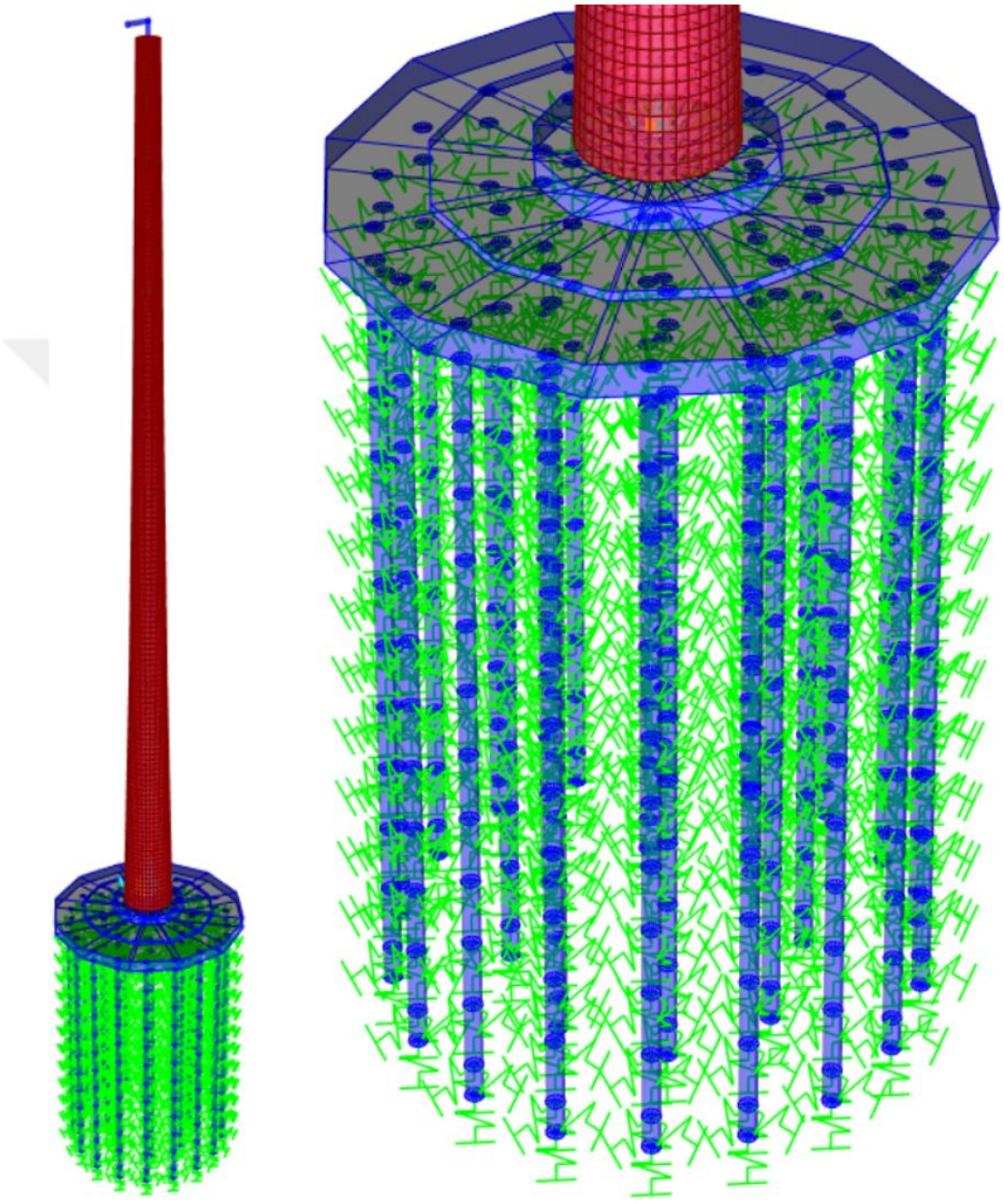

Figure 2.9. Finite Element Model of the Wind Turbine including Foundation and Soil Springs.

2.3. FEM Updating

Aiming to minimize the difference between identified modal parameters of the wind turbine found by Enhanced Frequency Decomposition method and obtained modal parameters from the finite element model, finite element modal updating is performed. In the FEM updating process, natural frequencies and mode shapes of the first 3 modes in each direction are considered. Modal identification of the wind turbine is out of the scope of this study therefore a previous work on the same wind turbine is taken as the reference for identified modal parameters [48].

For the FEM updating process, steel Young's modulus and soil spring coefficients are chosen as updating parameters. In this scope, 21 different cases for steel Young's modulus ranging between 180 GPa and 220 GPa and 19 different cases for soil spring coefficients ranging between 20% and 200% of calculated values are considered. A total of 399 analyses are performed for each combination of these parameters. For each analysis, natural frequencies and mode shapes of the first three modes in each direction are recorded. The differences between identified modal parameters and obtained modal parameters from the finite element model are investigated with an error function defined in MATLAB. The error function used in FEM updating considering natural frequencies and mode shapes is given below.

$$Er = \sum \left[k_i \times \left[\frac{f_i^* - f_i}{f_i^*} \right]^2 + h_i \times [1 - MAC_i]^2 \right] \tag{2.11}$$

where

Er : Error function

k_i : Weighting coefficient for natural frequencies for mode i

f_i^* : Identified natural frequency for mode i

f_i : Obtained natural frequency from finite element model for mode i

h_i : Weighting coefficient for mode shapes for mode i

MAC_i : Modal assurance criterion for mode i

The modal assurance criterion (MAC) value given in the above equation is used to show the similarity between identified mode shapes and mode shapes found from the finite element model. The modal assurance criterion value is calculated with the equation provided below.

$$MAC = \frac{|\Psi_*^T \times \Psi|^2}{(\Psi_*^T \times \Psi_*) \times (\Psi^T \times \Psi)} \tag{2.12}$$

where

Ψ_*: Identified mode shape

Ψ : Obtained mode shape from finite element model

Weighting coefficients used in the error function are obtained according to the effective modal masses of the first three modes which are found from the finite element model. Analysis results show that effective modal masses of the first three modes are 0.58, 0.16, and 0.08 accordingly. Since only the first three modes are considered, each of these values are normalized with the total of these values. Weighting coefficients used in the error function are given in Table 2.12.

Table 2.12. Weighting Coefficients Used in Error Function.

Mode Number	**Weighting Coefficients for Natural Frequencies (k_i)**	**Weighting Coefficients for Mode Shapes (h_i)**
1	0.7	0.7
2	0.2	0.2
3	0.1	0.1

For the fore-aft direction case, the error function created according to the equation above takes minimum error value when soil spring coefficients are 40% of the calculated values and steel Young's modulus is 192 GPa. For side-to-side direction, error function gives minimum error when soil spring coefficients are 50% of calculated values and steel Young's modulus is 192 GPa. Both error matrices are investigated

and the combination giving minimum total error is chosen as the final model which is 50% of calculated soil springs and 192 GPa of steel Young's modulus. Error functions found for each direction are given in Figure 2.10 and Figure 2.11. The comparison of identified natural frequencies and obtained natural frequencies is provided in Table 3.2. Also, comparisons mode shapes are given in Figure 2.12 and Figure 2.13.

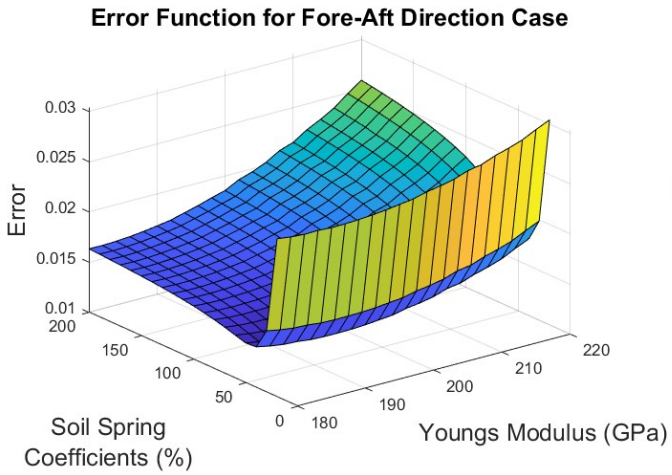

Figure 2.10. Error Function for Fore-Aft Direction Case.

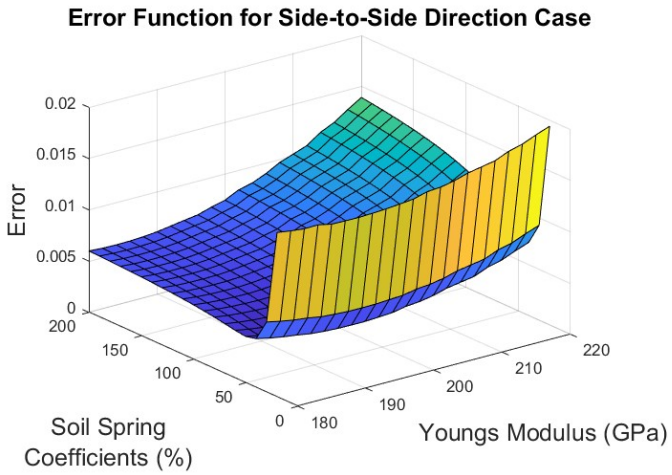

Figure 2.11. Error Function for Side-to-Side Direction Case.

Table 2.13. Natural Frequency Comparison.

Mode	Natural Frequencies of Initial Model (Hz)	Natural Frequencies of Updated Model (Hz)	Identified Natural Frequencies (Hz)
Fore-Aft Direction – 1st Mode	0.48	0.47	0.47
Fore-Aft Direction – 2nd Mode	3.51	3.28	3.30
Fore-Aft Direction – 3rd Mode	10.03	9.71	9.31
Side-to-Side Direction – 1st Mode	0.48	0.47	0.46
Side-to-Side Direction – 2nd Mode	3.48	3.26	3.31
Side-to-Side Direction – 3rd Mode	9.72	9.40	9.37

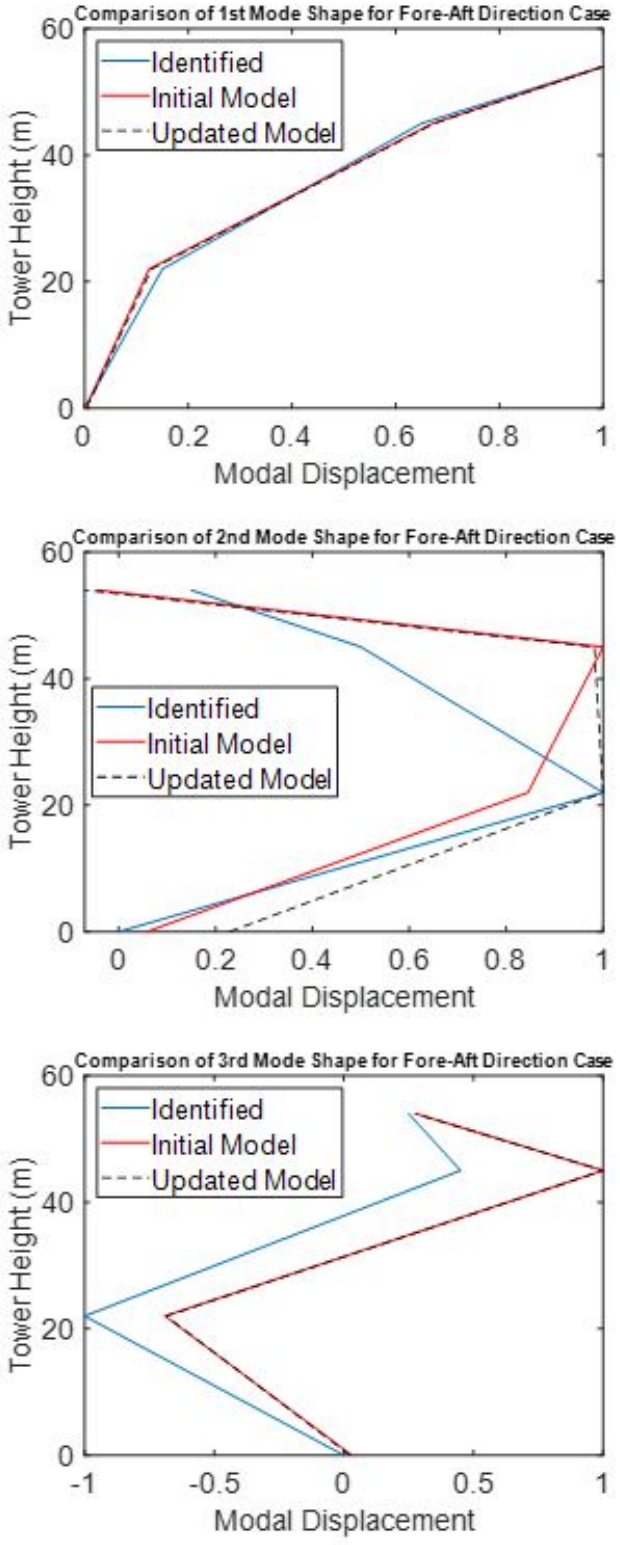

Figure 2.12. Mode Shape Comparison for Fore-Aft Direction Case.

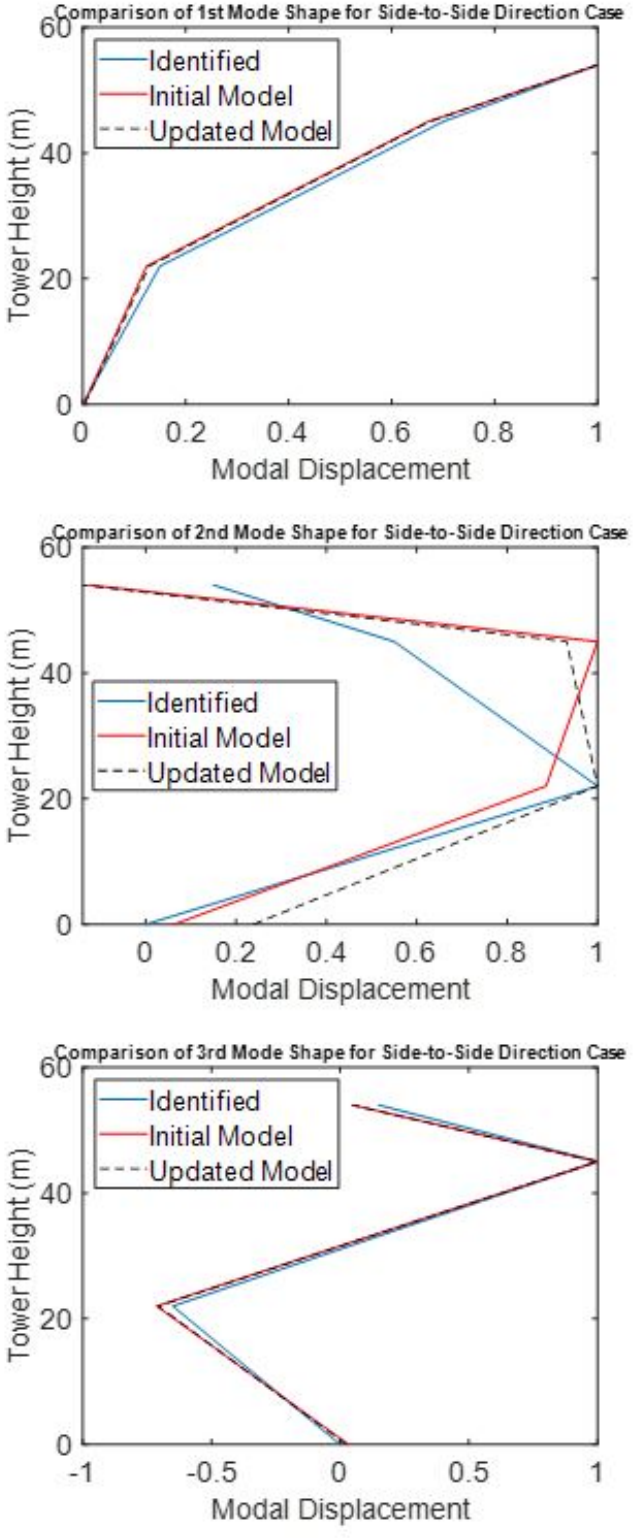

Figure 2.13. Mode Shape Comparison for Side-to-Side Direction Case.

3. PERFORMANCE ASSESSMENT

3.1. Pushover Analysis

A nonlinear finite element model of the wind turbine which considers both material and geometric nonlinearities is developed in ANSYS software to perform pushover analysis. The model is developed with shell elements. The Young's modulus of structural steel (S355) is taken as 192 MPa as found in the FEM updating process, the yield stress is taken as 355 MPa and the ultimate strength of steel is taken 470 MPa. The stress-strain diagram of the steel is assumed to be bilinear where ultimate strain is taken as 100 times of the yield strain. The stress-strain diagram used in the model is given in Figure 3.1.

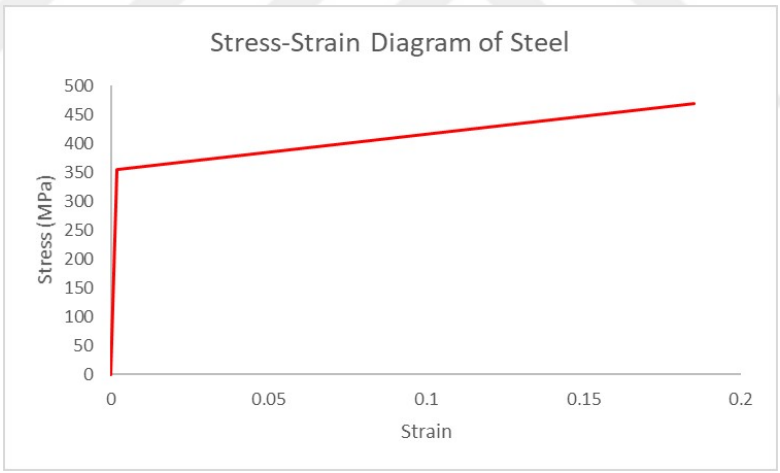

Figure 3.1. Stress-Strain Diagram of Structural Steel.

The total mass of the nacelle and rotor parts is assigned to the coordinates of the center of mass of these parts which is given in the design specifications of the wind turbine. The center of mass of these parts is 0.85 m above the top of the tower and 1.52 m away from the center of the tower in the horizontal direction. This point mass representing the rotor and nacelle parts is attached to the top edge of the wind turbine.

For the structural damping of the wind turbine, the Rayleigh damping approach is used. Mass and stiffness coefficients obtained according to this approach are defined in the model. The Rayleigh damping as a function of stiffness and mass matrices is defined as [49]:

$$[C] = a_0[M] + a_1[K] \tag{3.1}$$

where

a_0 : mass coefficient

a_1 : stiffness coefficient

Mass and stiffness coefficients given in above equation are defined for the damping ratio of a specified mode of vibration as

$$\zeta_n = \frac{a_0}{2}\frac{1}{w_n} + \frac{a_1}{2}w_n \tag{3.2}$$

where

ζ_n : Specified damping ratio of mode n

w_n : Natural frequency of mode n (Hz)

Using the equation above for 2 different modes of vibration, and putting them in matrix form, the following relationship is obtained.

$$\frac{1}{2}\begin{bmatrix} 1/w_i & w_i \\ 1/w_j & w_j \end{bmatrix}\begin{Bmatrix} a_0 \\ a_1 \end{Bmatrix} = \begin{Bmatrix} \zeta_i \\ \zeta_j \end{Bmatrix} \tag{3.3}$$

For the calculations, damping values and natural frequencies of the first 2 modes which are identified as 4.36% and 4.15% respectively are used [48]. Mass and stiffness coefficients calculated according to the above equations using identified damping ratios of the first 2 modes and defined in the finite element model are given in Table 3.2.

Table 3.1. Mass and Stiffness Constants.

a_0	a_1
0.0411	0.0265

In order to consider the soil flexibility effects on structural behavior, global soil springs are used. Stiffness values of global springs are determined by applying virtual loads to the top of the detailed foundation model including pile cap, piles, and API soil springs in the corresponding degree of freedoms. In this process, API spring coefficients found in the FEM updating section are used which are 50% of initially calculated stiffness values. Finally, displacement and rotation demands for each degree of freedom are recorded and stiffness values of global springs are calculated. At this point, natural frequencies of first 3 modes of vibration obtained by the ANSYS model are compared with natural frequencies obtained by the updated SAP2000 model and it is seen that both models give similar results that verifies the validity of the model developed in ANSYS software. The nonlinear model developed in ANSYS considering soil flexibility by global springs is given in Figure 3.2.

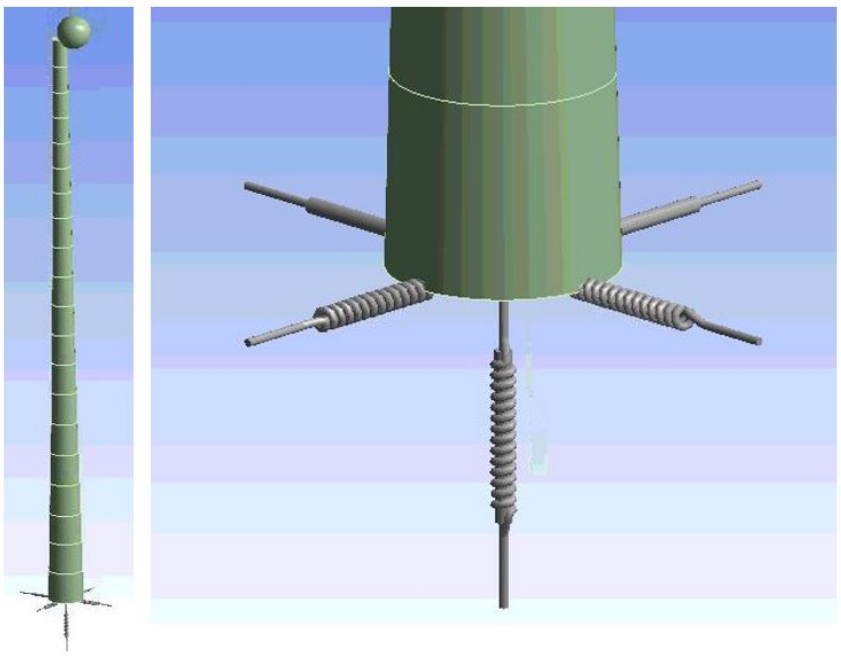

Figure 3.2. Nonlinear Model Developed in ANSYS.

After the verification of the nonlinear finite element model, two displacement-controlled pushover analyses of the wind turbine are conducted with and without considering the dead load coming from nacelle and rotor parts to investigate the effects of including these part on the pushover analysis. In the first case, only lateral top displacement is applied to the steel tower of the wind turbine incrementally. In the second case, dead load analysis of the structure is performed prior to the pushover analysis which already creates a similar stress distribution with the pushover analysis where lateral top displacement is applied in the fore-aft direction. The eccentric location of the center of mass of rotor and nacelle parts causes slight pre-stresses on the structure. Also, initial dead load analysis leads to a base shear in the same direction of lateral displacement which causes the pushover curve of the case with the dead load starting from a negative value. Pushover curves with and without considering dead load effect of nacelle and rotor parts are provided in Figure 3.3

.

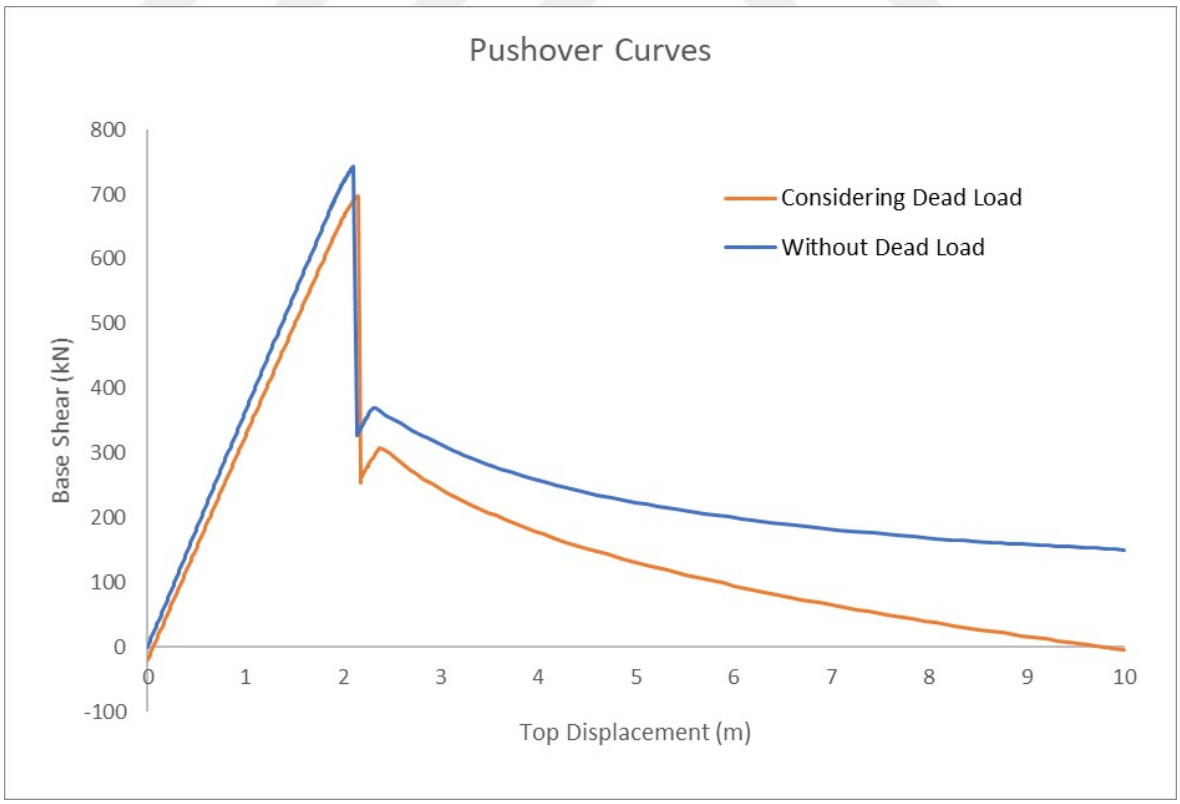

Figure 3.3. Pushover Curves.

Pushover analysis results show that considering the dead load of nacelle and rotor parts influences the structural response and causes approximately 6% decrease in base shear capacity of the wind turbine. Results also show that both pushover curves are almost perfectly linear before buckling and a slight nonlinearity is seen in the last few iterations of the pushover analysis just before buckling. At the steps where buckling occurs, sudden drops which are around 60% of ultimate base shear capacities are seen in the base shear capacities for each case. After the occurrence of buckling, base shears decrease gradually in both cases. The pushover curve in which dead load is considered reaches zero at the lateral displacement of 10 m while the one without dead load action decreases to around 150 kN at the same lateral displacement. Also, deformed shapes and stress distributions of the tower at just before buckling, just after buckling and at the final step are provided in Figure 3.4.

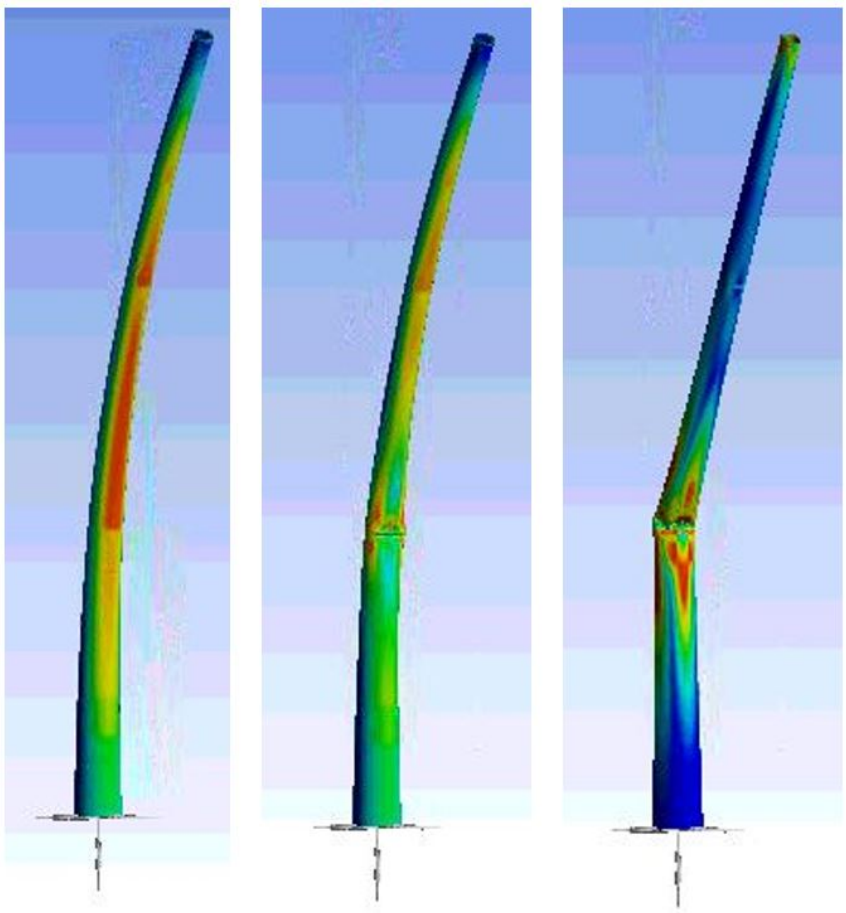

Figure 3.4. Stress Distributions at Different Steps of Pushover Analysis.

The wind turbine is susceptible to have local imperfections on the steel tower therefore the influence of initial geometric imperfections on the buckling capacity of the steel tower is also investigated. For this purpose, an initial geometric imperfection is defined in the model by performing linear buckling analysis prior to the pushover analysis to define virtual initial imperfection to the wind turbine model. The model is analyzed for different scales of initial geometric imperfections. The initial geometric imperfection defined for scale 20 which results in 20 mm imperfection is given in Figure 3.5.In this part, the pushover analysis which considers the dead load effect coming from nacelle and rotor parts is used.

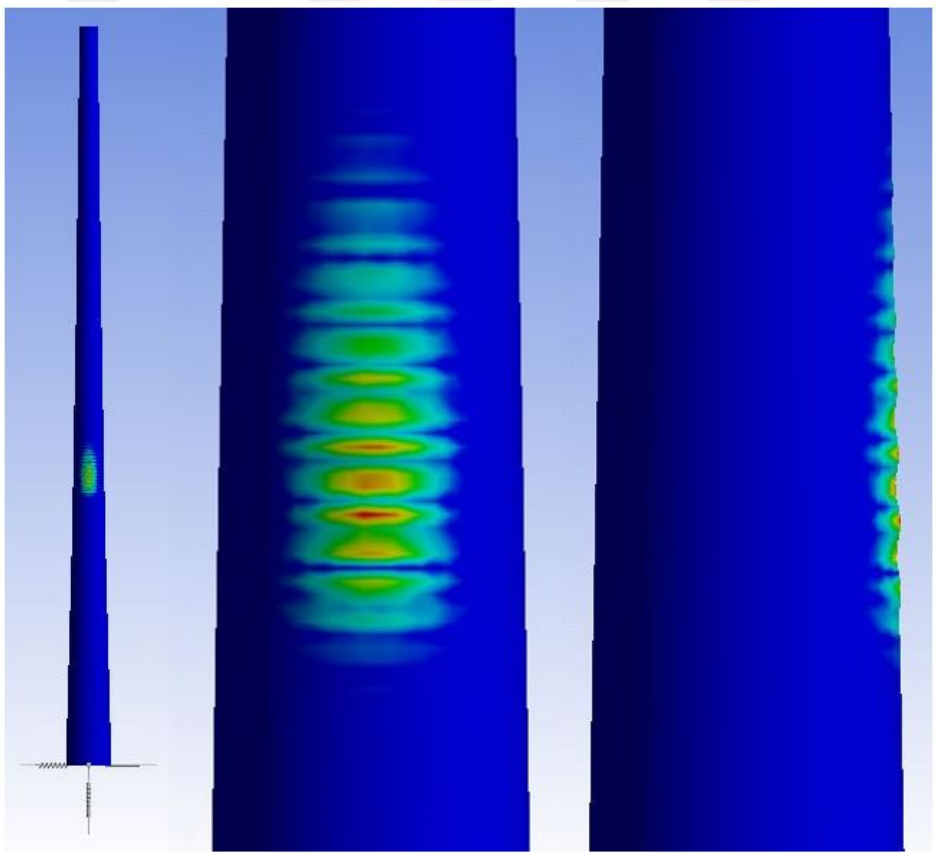

Figure 3.5. Initial Imperfection Defined in the Model.

Pushover curves for ignoring initial geometric imperfection and considering five different initial geometric imperfection scales are provided in Figure 3.6. Pushover analysis results show that initial geometric imperfection may have a significant effect

on the buckling capacity of the structure. Even in the 1 mm initial imperfection case, the decrease in the buckling capacity of the tower can be seen clearly in the pushover curves plot. In the 5 mm initial imperfection case, the buckling capacity decreases approximately 20% while it decreases around 35% in the case with 20 mm initial geometric imperfection. It is also seen from the results that the buckling capacity decreases as the scale of initial geometric imperfection increases as expected.

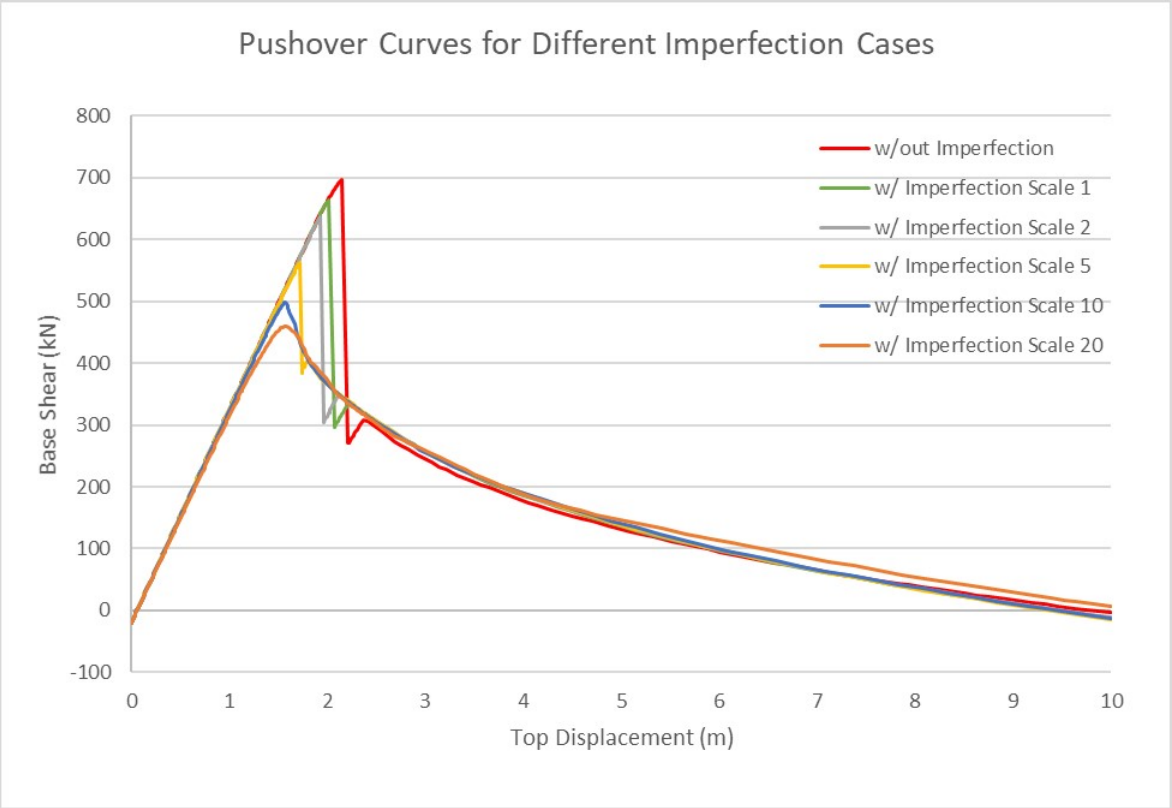

Figure 3.6. Pushover Curves for Different Imperfection Cases.

3.2. Demand-Capacity Spectrum Approach

After the pushover analysis is completed, the capacity curve is developed by the conversion of the pushover curve into the capacity curve procedure. Effective modal mass and participation factor values are calculated assuming that the total mass of steel tower is lumped at 20 discrete levels where the sum of the masses of hub and nacelle is added to the top level. For the verification of this assumption, modal anal-

ysis of the wind turbine model is performed in SAP2000 software and the parameters obtained from the FEM are compared with calculated values. Results show that analytically obtained values coincide with SAP2000 results which verifies the correctness of our assumption. Effective modal masses and modal participation factors for the first mode found according to the simplified approach and obtained from the finite element model are given in Table 3.2.

Table 3.2. Effective Modal Mass and Modal Participation Factors for the First Mode.

	SAP2000 Results	**Calculated Values**
Effective Modal Mass	0.58	0.59
Modal Participation Factor	6.87	7.15

The vertical axis of the pushover curve is converted into spectral acceleration values which are calculated according to the following equation.

$$A_1 = V_1/M_{x1} \tag{3.4}$$

where

V_1 : Base shear (kN)

M_{x1} : Effective modal mass of first mode

$$M_{x1} = \frac{L_{x1}^2}{M_1} \tag{3.5}$$

where

$$L_{x1} = \sum m_i * \Phi_{xi,1} \tag{3.6}$$

$$M_1 = \sum m_i * \Phi_{xi,1}^2 \tag{3.7}$$

The horizontal axis of the pushover curve is converted into spectral displacement values which are calculated with the following equation.

$$d_1 = \frac{U_{top,1}}{\Phi_{top,1} \times \Gamma_1} \tag{3.8}$$

where

$U_{top,1}$: Displacement demand at the top of the tower (m)

$\Phi_{top,1}$: First mode shape amplitude at the top of the tower

Γ_1 : Participation factor for the first mode

$$\Gamma_1 = \frac{L_{x1}}{M_1} \tag{3.9}$$

The capacity curve obtained from pushover curve with the equations provided above is given in Figure 3.7.

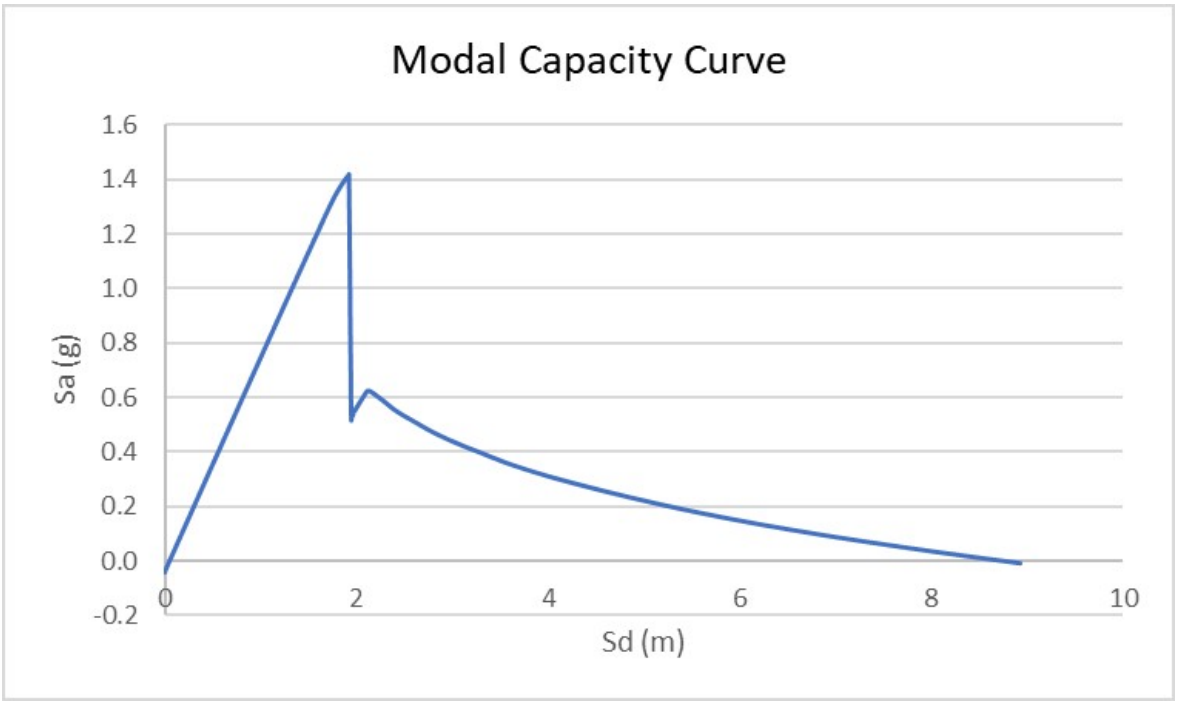

Figure 3.7. Modal Capacity Curve.

Then, the elastic design spectrum is obtained for the site of the wind turbine tower according to the 2018 Turkish Seismic Code for local soil class ZD which represents soil with dense-medium dense sand and stiff clay. Ground motion level 2 which represents ground motions with an exceedance probability of 10% percent within 50 years is selected for the design spectrum. The design obtained for the wind turbine site is given in Figure 3.8.

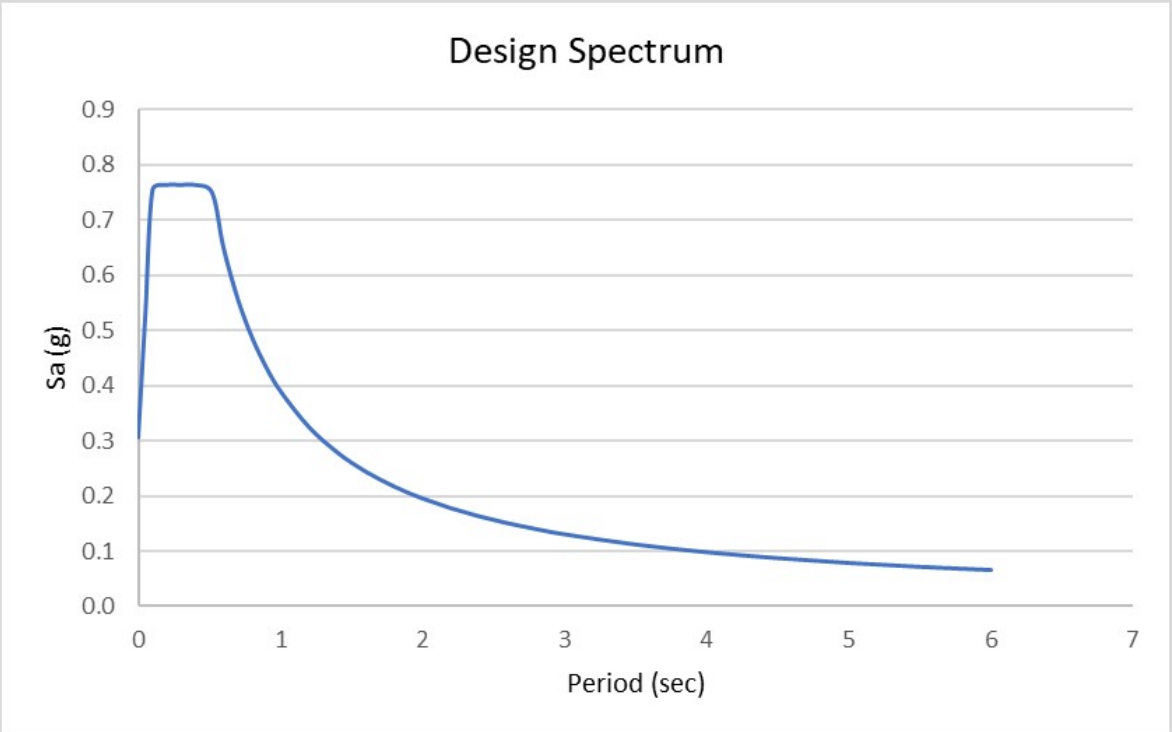

Figure 3.8. Design Spectrum.

The elastic design spectrum is converted to demand curve according to the relationship between spectral acceleration and spectral displacement given below.

$$S_d = \frac{S_a}{w_1^2} = \frac{S_a}{(2\pi/T_1)^2} \tag{3.10}$$

In this conversion, equal displacement rule is applied since the wind turbine tower is a flexible structure and has a very high natural period for the first mode of vibration. The modal displacement demand curve is given in Figure 3.9.

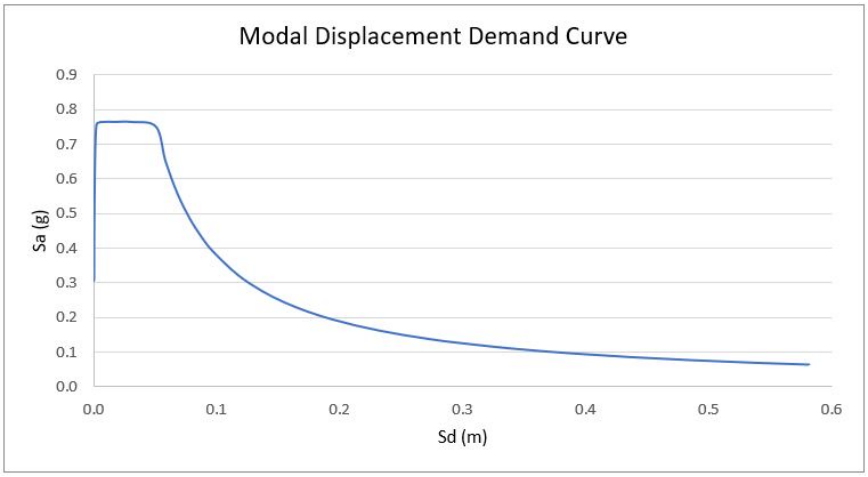

Figure 3.9. Modal Displacement Demand Curve.

The comparison of demand and capacity curves is provided in Figure 3.10. Spectral acceleration at the performance point which is the intersection of the modal capacity curve and modal displacement curve is 0.16 g while spectral displacement value at this point is 240 mm. This means that expected top displacement demand under a probable earthquake is 240 mm which is approximately 12% of displacement value causing buckling of the structure. This result shows that the wind turbine meets the performance criteria determined according to this approach.

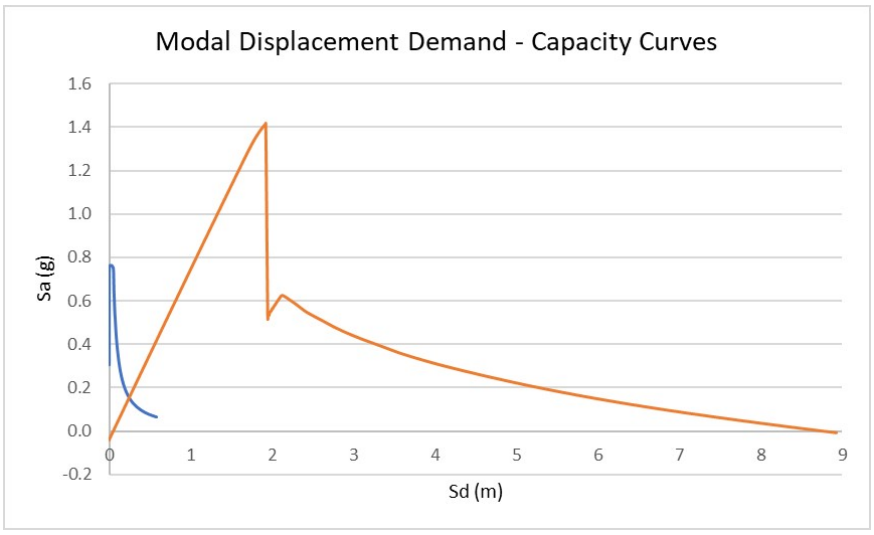

Figure 3.10. Comparison of Demand and Capacity Curves.

3.3. Seismic Fragility Analysis

Fragility curves represent the probability of reaching or exceedance a determined damage state of an engineering demand parameter at the corresponding intensity measure level. They are statistical tools used to predict the vulnerability and reliability of a structure under seismic actions. Fragility curves are developed by plotting a two-parameter lognormal cumulative distribution function according to the damage reports obtained from the incremental dynamic analysis with selected ground motions. The intensity measure for the fragility analysis can be several parameters like SA, SV, SI, PGA, PGV, etc. For this study, the buckling of the steel tower of the wind turbine is chosen as the engineering demand parameter and spectral acceleration for the first mode is taken as the intensity measure.

The two-parameters used in the development of fragility curves are determined by the maximum likelihood procedure. The equation of the maximum likelihood function is given below [50].

$$L = \prod_{i=1}^{N} [F(a_i)]^{x_i} [1 - F(IM_i)]^{1-x_i} \tag{3.11}$$

where

$F(.)$: Fragility curve for a specific state of damage

IM_i : Intensity measure values

x_i : Damage case (1 for damaged, 0 for undamaged)

N : Number of ground motions

The fragility curve is defined as a lognormal cumulative distribution function. The fragility function used in the maximum likelihood function has the form which is provided below.

$$F(a) = \Phi \left[\frac{ln(IM/med)}{s} \right] \tag{3.12}$$

where

$\Phi[.]$: Standardized normal distribution function

IM : Intensity measure

med : Median

s : Log standard deviation

The two-parameters med and s are computed by maximizing the maximum likelihood function which can be formalized as below.

$$\frac{d(ln(L))}{d(med)} = \frac{d(ln(L))}{d(s)} = 0 \tag{3.13}$$

For the development of the fragility curve, incremental dynamic analysis is performed with several ground motions and damage report is obtained. Incremental dynamic analysis of the wind turbine model is performed with 11 earthquake records which are compatible with the design spectrum of the structure obtained before. In the earthquake selection procedure, both the compatibleness of the geometric mean of selected earthquakes with the design spectrum and the compatibleness of each earthquake record with the design spectrum are aimed. As the intensity measure of the fragility curve, spectral acceleration for the first mode is selected. In the analyses, spectral acceleration values at 2.15 seconds which is the natural period of the first mode of the wind turbine are scaled for all ground motions records. The comparison of the design spectrum with the geometric mean of earthquake records is given in Figure 3.11 and the comparison of the design spectrum with every ground motion record is given in Figure 3.12.

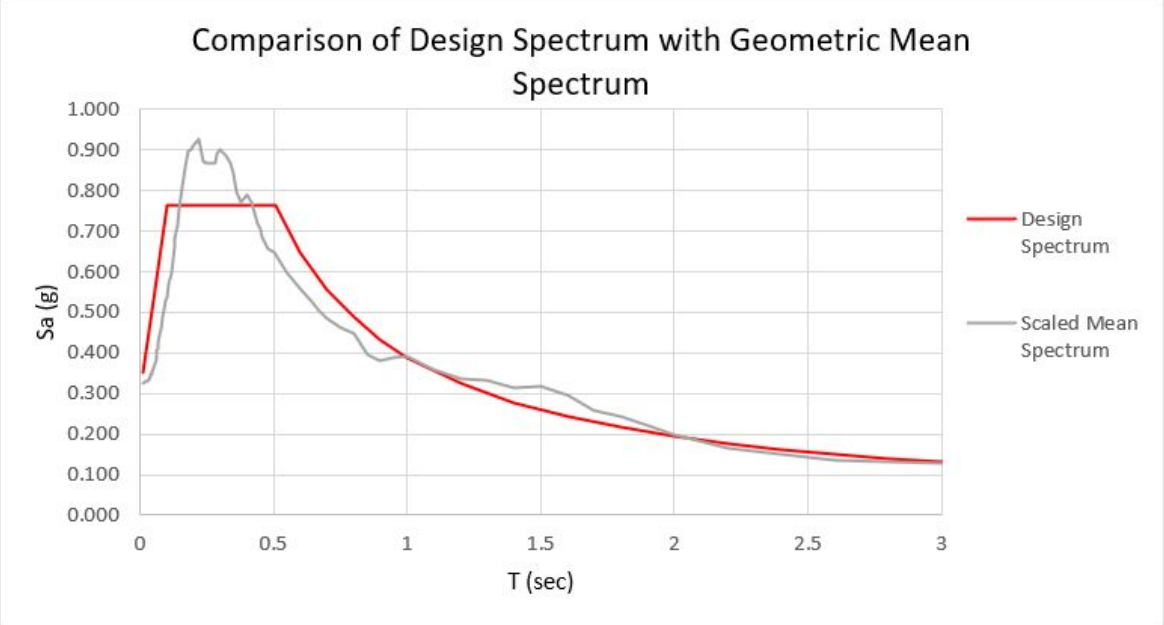

Figure 3.11. Comparison of Design Spectrum with Geometric Mean Spectrum.

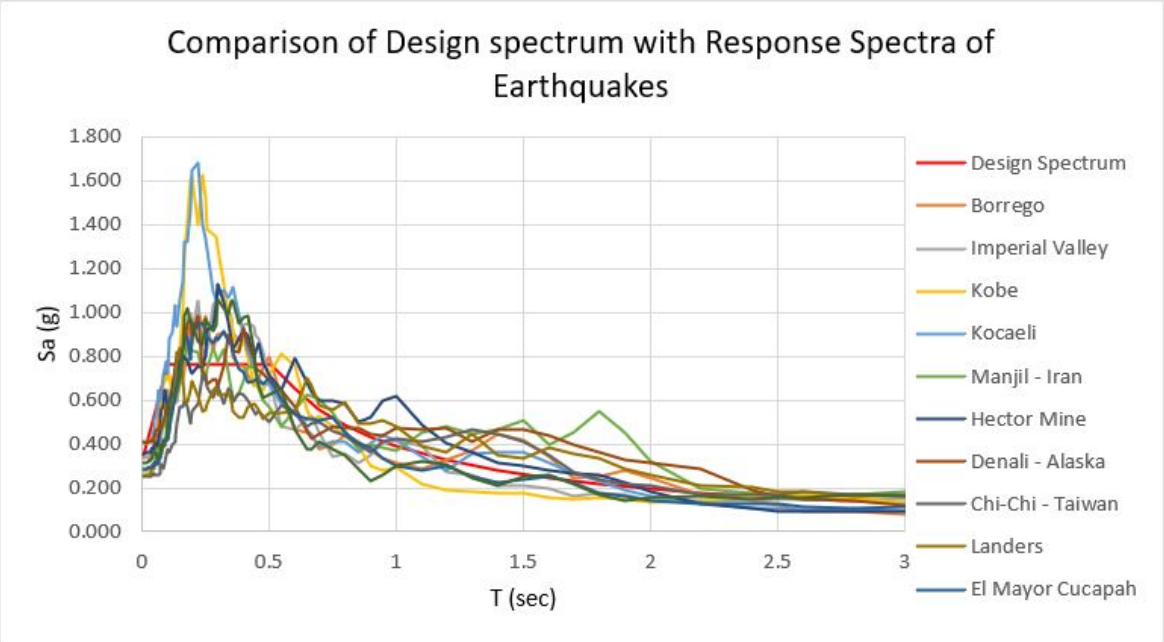

Figure 3.12. Comparison of Design Spectrum with Response Spectra of Earthquakes.

In the fragility analysis, wind load action which has significant effect on the structural performance is also considered. For the wind loading, TurbSim and FAST softwares are used. TurbSim software simulates three-dimensional stochastic, full-field and turbulent wind speed times histories at pre-determined points on a two-dimensional vertical wind field which is fixed in the space. It numerically generates wind speed time histories for mean wind speed and turbulence intensity parameters. IEC von Karman spectrum is used in the generation of wind speed time histories. Visual representation of wind field used in TurbSim software is given in Figure 3.13 [51].

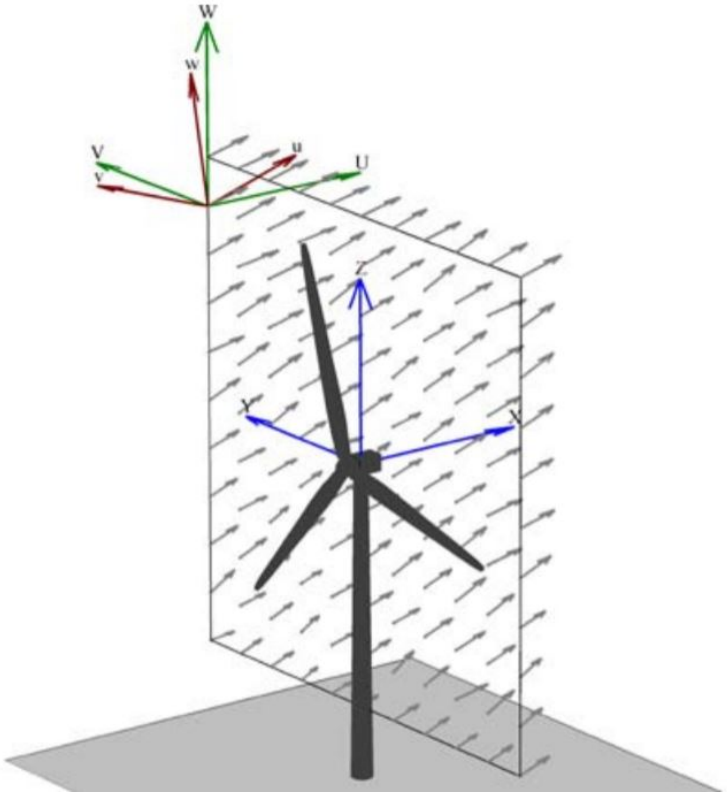

Figure 3.13. Visual Representation of Wind Field [51].

FAST is an aeroelastic simulation program which carries out dynamic analysis of wind turbines under wind loading. Wind speed time histories obtained in the TurbSim software and modal parameters of the wind turbine obtained in the SAP2000 model are transferred to the FAST software and aerodynamic load time histories at the rotor level are predicted [52].

In the scope this study, wind speed time histories for 5 m/s, 15 m/s and 25 m/s mean speed levels are used. The one with 5 m/s mean speed is classified as gentle breeze according to the Beaufort Scale which causes slight excitation of the wind turbine tower. The wind with 15 m/s mean speed is classified as high wind which causes significant excitation demands on the structure. The latest one with 25 m/s mean speed is classified as storm or whole gale that leads extreme rotor thrust demands on the wind turbine tower [53]. Turbulence intensity values of all wind speed time histories are selected as 13%. Wind loading time histories obtained from FAST software at the rotor level are provided in Figure 3.14.

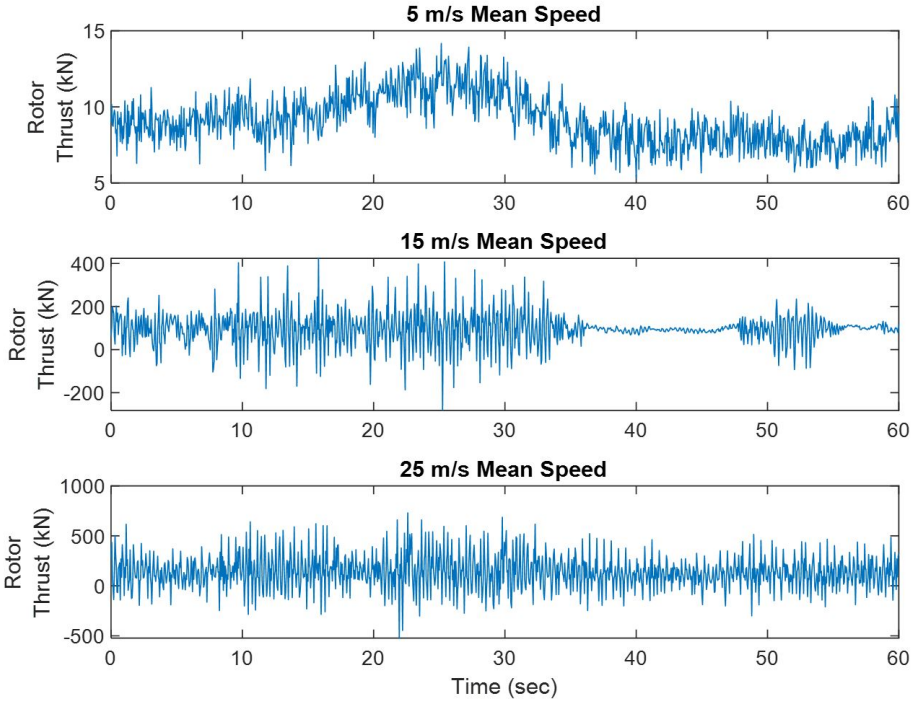

Figure 3.14. Rotor Thrust Time Histories obtained from FAST.

Fragility curves considering the wind load time histories provided above and without considering wind action are developed. Dynamic analyses of the wind turbine for spectral acceleration increments are performed with the finite element model developed in SAP2000 software. At this point, pushover analysis results obtained in the ANSYS model is taken as reference. Pushover analysis results show that steel tower of the wind turbine buckles when the minimum principle stress on the tower reaches

approximately -392 MPa where minus sign indicates compression. So, this stress value is taken as buckling stress threshold and spectral acceleration increments that cause the structure have equal or higher than the buckling stress threshold are labeled as damaged and damage report is completed for fragility curve development. Fragility curves developed for different mean wind speeds are given in Figure 3.15.

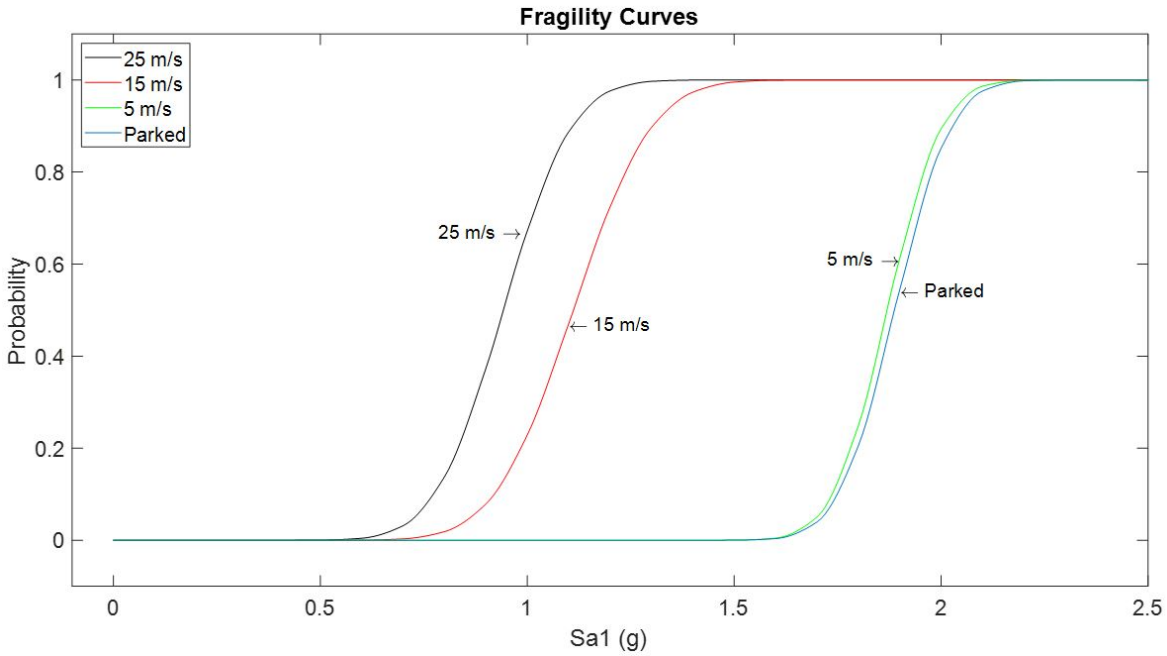

Figure 3.15. Fragility Curves.

Fragility curves show that minimum spectral accelerations leading buckling stress are 1.8g for parked condition without any wind load action and for the wind action with 5 m/s mean speed. This shows that gentle breeze does not have a considerable influence on the structural performance. Also, it is seen that very high spectral acceleration demands are needed in both cases for the buckling of the steel tower. On the other hand, the buckling of the steel tower becomes probable when spectral acceleration reaches 0.9g for 15 m/s mean wind speed case and reaches 0.8g for 25 m/s mean speed wind case. These results are very important because 15 m/s wind speed equals approximately to the rated wind speed at which the wind turbine generates electricity at its maximum capacity. So, this demonstrates that wind action needed for the maximum electricity generation has a significant influence on the structural performance of the wind turbine.

4. RESONANCE PHENOMENON

In the performance assessment of the wind turbine, only wind and earthquake loads are considered as excitation sources. But for wind turbines, also resonance phenomenon which occurs due to the rotation of wind turbine blades may become an important source of excitation and lead to severe structural demands. In this scope, concepts of mass unbalance and tower dam effects are discussed and the influence of the resonance phenomenon on the structural behavior are investigated.

The blades of the wind turbine rotate as the wind flows through. However, when the location of a blade intersects with the wind turbine tower, the tower becomes an obstacle to the wind and blocks the flow. In this way, the periodic excitation of the wind turbine tower occurs. The frequency of the periodic excitation is n*Ω where n represents the number of blades and Ω represents the rotational frequency of blades. The wind turbine investigated in this study has three blades therefore the tower dam effect leads to periodic excitation with a frequency of 3*Ω and its multiples [54].

The rotation of wind turbine blades leads to the occurrence of centrifugal forces at the top. Having the same angular frequency, all blades cause the same centrifugal forces when the masses of all blades are equal and no excitation occurs. However, mass unbalance may occur due to manufacturing defects or water intrusion to one of the blades [56]. In the mass unbalance case, the excess mass causes a periodic excitation where the excitation frequency equals to the angular frequency of the rotation of blades. When the frequency of this excitation meets with the natural frequency of the wind turbine tower, resonance may occur, and this small excitation may lead to significant structural demands [55].

Expected influences of resonance phenomenon on the structural response are provided in Figure 4.1 [55]. It's seen that the resonance phenomenon leads to significant increase in tower amplitude.

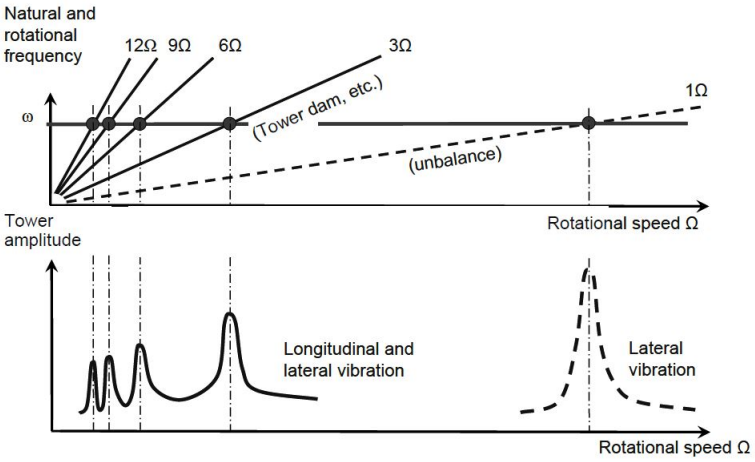

Figure 4.1. Resonance Peaks [55].

In order to investigate the resonance phenomenon, the Campbell diagram of the wind turbine is generated. Campbell diagram illustrates the relationship between the exciting frequencies, natural frequencies of the structure, and the rotational speed of blades. Also, the operating range of the wind turbine is defined in the Campbell Diagram. The lower limit of the operating range is cut-in rotor speed which is given as 16 rpm and the upper limit is cut-out rotor speed which is given as 34.5 rpm in the design specifications. The Campbell diagram of the wind turbine is given in Figure 4.2.

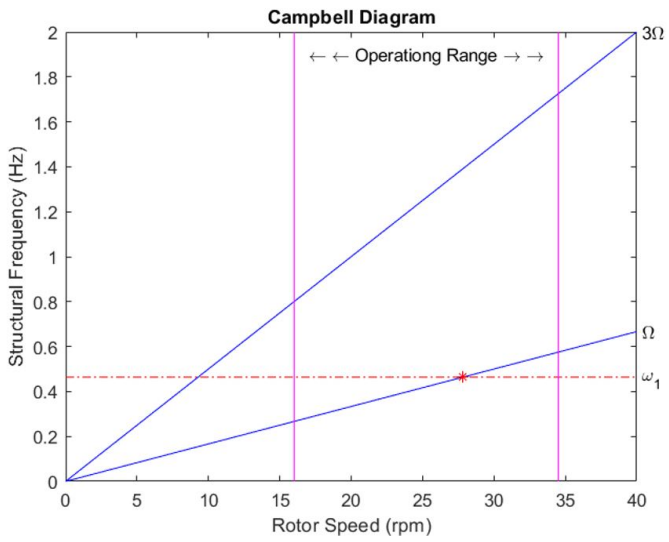

Figure 4.2. Campbell Diagram.

It is seen from the Campbell diagram that the fundamental frequency of the structure matches the exciting frequency due to mass unbalance when the rotor speed is equal to 27.8 rpm which falls between the operating range limits. So, a 50-min acceleration time history data is examined in a time range while the rotor speed gets the value of 27.8 rpm to see whether resonance occurs and causes an additional excitation. The comparison of acceleration time history at the top level of the wind turbine and rotor speed time history for the same time interval is given in Figure 4.3.

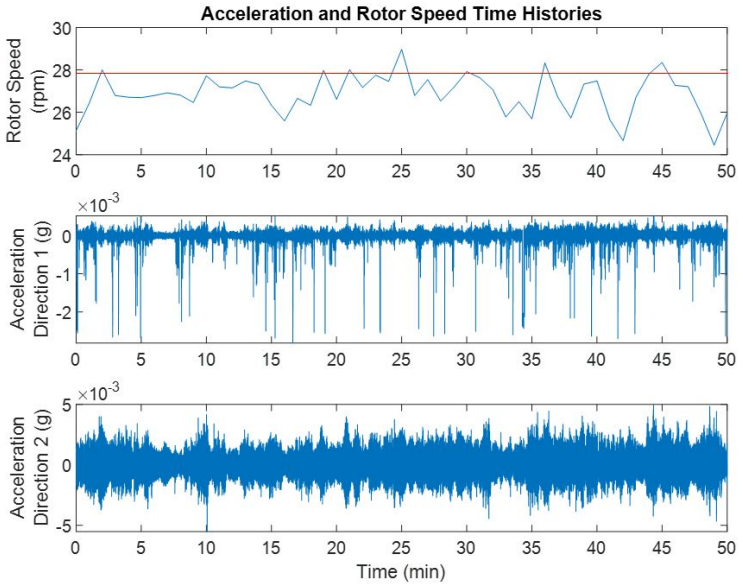

Figure 4.3. Comparison of Acceleration and Rotor Speed Time Histories.

It is seen from the Figure 4.3 that the tower doesn't experience an additional excitation due to the resonance effect when rotor speed matches the fundamental frequency. This is probably due to the homogeneous mass distribution of wind turbine blades, in other words, there is no mass unbalance because of manufacturing inaccuracies. Also, in the design specifications of the wind turbine, it is claimed that the control system of the wind turbine prevents it from unexpected conditions like high temperature or high level of vibrations via control sensors. This may also be the reason why resonance peaks are not seen in the structure. So, it is seen that resonance phenomenon is prevented in this wind turbine and it is not necessary to consider it as an additional source of excitation.

5. CAPACITY CHECKS

In the literature, there are also analytical calculations for buckling capacities. In order to check the validity of these approaches, the analytical buckling capacity of the wind turbine is compared with time history analysis demands.

The analytical buckling capacity of the wind turbine tower considering the local buckling effects is calculated according to two different references which are AISC's Specification for Structural Steel Buildings and Ziemian's Guide to Stability Design Criteria for Metal Structures [57,58]. The steel tower of the wind turbine is subjected to flexure under lateral loads and the buckling capacity of round hollow structural sections (HSS) subjected to flexure is given in terms of moment capacity in both references.

5.1. Specification for Structural Steel Buildings (AISC, 2016)

In the AISC Specification, sections of structural elements subjected to flexure are classified as compact, noncompact, and slender sections for consideration of local buckling. These section classes are determined according to two limiting width-to-thickness ratios which are λ_p and λ_r. These parameters for the round HSS sections are calculated according to the equations given below.

$$\lambda_p = 0.07\frac{E}{F_y} \tag{5.1a}$$

$$\tag{5.1b}$$

$$\lambda_r = 0.31\frac{E}{F_y} \tag{5.1c}$$

where

E = Young's Modulus (MPa)

F_y = Yield Stress (MPa)

Sections having diameters to thickness ratios smaller than λ_p are labeled as compact sections where local buckling does not apply, and complete yielding occurs. For compact sections, the buckling capacity of the round HSS section is calculated according to the equation given below.

$$M_n = F_y \times Z \tag{5.2}$$

where

Z: Plastic Section Modulus (m^3)

Sections having a diameter to thickness ratios greater than λ_p but lower than λ_r are labeled as noncompact sections. Local buckling occurs in noncompact sections and the buckling capacity of the element decreases. The buckling capacity of noncompact round HSS sections under flexure is calculated by the equation provided below.

$$M_n = \left[\frac{0.021E}{D/t_w} + F_y\right] S \tag{5.3}$$

where

D : Outside diameter of round HSS (m)

t_w : Design wall thickness (mm)

S : Elastic section modulus (m^3)

Sections with diameter to thickness ratios greater than λ_r value are defined as slender sections which are also susceptible to the local buckling occurrence. For the slender round HSS sections, the buckling capacity considering local buckling is calculated according to the equation given below.

$$M_n = F_{cr}S \tag{5.4}$$

where

$$F_{cr} = \frac{0.33E}{D/t_w} \tag{5.5}$$

The wind turbine has varying thickness and diameter values along with the height. For this reason, the diameter to thickness ratios of cross-sections of the wind turbine tower are calculated with 10 cm intervals and labeled according to the classification defined above. All sections of the wind turbine are found as noncompact sections therefore the buckling capacity of the wind turbine is calculated according to the equation 5.3 for all sections.

5.2. Guide to Stability Design Criteria for Metal Structures (Ziemian)

For the inelastic buckling capacity of tubular steel structures subjected to flexure, experimental data of previous studies is presented. A linearized best-fit curve of the data is indicated. Experimental data and linearized best-fit curve plot provided in this reference is given in Figure 5.1.

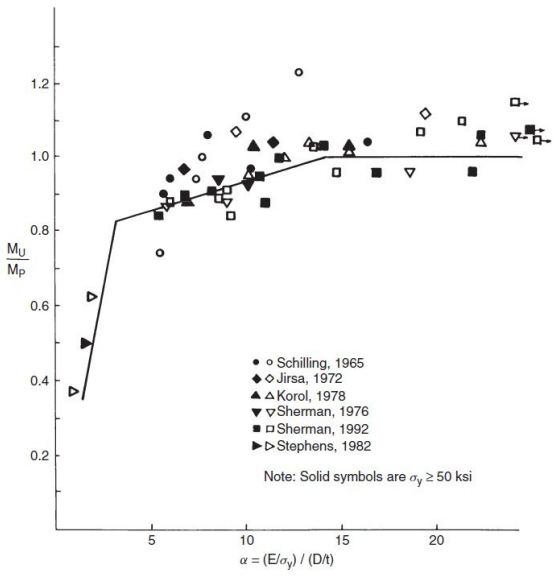

Figure 5.1. Experimental Data for Moment Capacity [58].

This best-fit curve can be formulized with the equations given below.

$$\frac{M_u}{M_p} = \begin{cases} 1 & \text{for } \alpha \geq 14. \\ 0.775 + 0.016\alpha & \text{for } \alpha < 14. \end{cases} \tag{5.6}$$

where;

M_u = Ultimate moment capacity (kN.m)

M_p = Plastic moment capacity (kN.m)

$$\alpha = \frac{E/\sigma_y}{D/t_w} \tag{5.7}$$

σ_y : Yield Stress (MPa)

The buckling capacities of the steel tower of the wind turbine are calculated along the height according to both approaches. It is seen that both approaches give similar results. Then, these capacities are compared with bending moment demands of earthquake analyses. Comparisons of bending moment demands of the wind turbine under several earthquakes with analytical capacities are provided in Figure 5.2 and Figure 5.3. It is observed that bending moment demands are almost linear under seismic actions which means the structure behaves like a single degree of freedom system. It is expected because the wind turbine has a slender structure and it has a concentrated mass on top of it which is approximately 40% of the total mass.

Comparison results show that the demand/capacity ratio converges to 1 at two different elevations where the buckling occurs at one of these points in the nonlinear analyses. Accordingly, this shows that analytically developed capacity calculations give reasonable results and can be used as a starting point for the performance assessment of wind turbines.

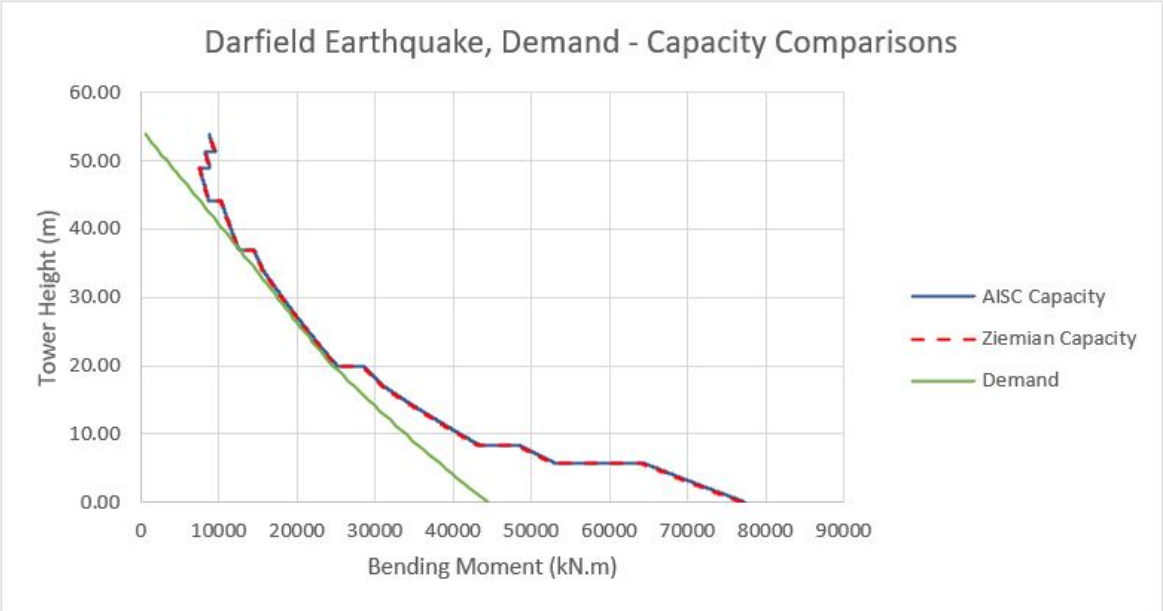

Figure 5.2. Bending Moment Demand under Darfield Earthquake and Analytical Capacities.

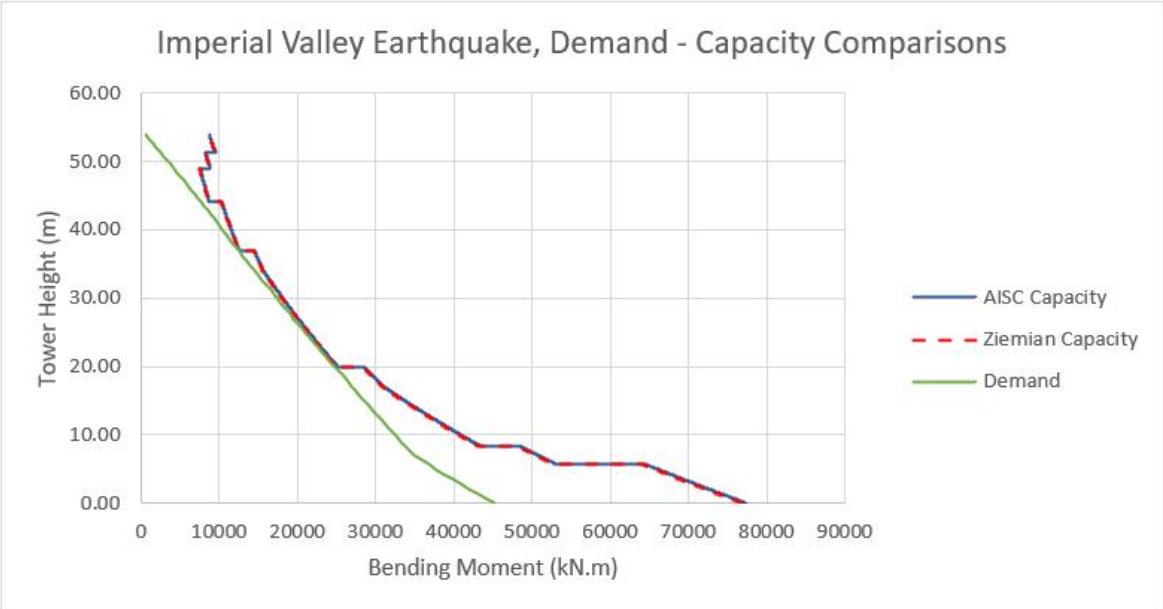

Figure 5.3. Bending Moment Demand under Imperial Valley Earthquake and Analytical Capacities.

6. CONCLUSION

In this study, the structural performance of the wind turbine in the Sarıtepe Campus of Boğaziçi University is investigated under seismic and wind loadings. A detailed finite element model of the wind turbine is developed in SAP2000 software. The steel tower of the wind turbine is modeled with shell elements to carry out a stress-based study and to properly model the thin-walled texture of the steel tower. In the FEM, soil flexibility is also considered. For this purpose, the foundation of the wind turbine including pile cap and piles is modeled according to the design specifications first. Then, soil springs that represent soil around piles are assigned to piles at discrete intervals. When the dynamic properties of two models with and without considering soil flexibility are compared, it is seen that considering soil flexibility influences dynamic properties of the structure i.e, a decrease is observed in natural frequencies and a slight change is observed in mode shapes of the structure when the foundation with soil springs is included in the model. But the dynamic parameters do not match perfectly with identified values therefore FEM updating is performed with two variables which are Young's modulus and soil spring coefficient percentage to minimize the difference between identified and obtained modal parameters. In the FEM updating, natural frequencies and mode shapes of the first three modes are considered. Error function surface is developed and the minimum error between identified and obtained modal parameters is seen for the case with 192 GPa steel Young's modulus and 50% of initially calculated soil spring coefficients. So, the final version of the model is developed using the values of two variables obtained in the FEM updating process.

In the FEM updating process, it is observed that the influence of the soil spring coefficient percentage on changes in the dynamic properties of the wind turbine is very limited. It is expected because the piled foundation of the wind turbine makes the structure behave almost like a fixed-based structure. Accordingly, a 50% decrease in soil spring coefficient does not have a significant influence on the dynamic properties of the structure since the influence of soil flexibility is limited.

A nonlinear pushover analysis of the wind turbine is performed. A nonlinear FEM of the wind turbine is developed in ANSYS software which considers both material and geometric nonlinearities. In the ANSYS model, soil flexibility is also considered which is modeled with global springs. The stiffnesses of global springs are obtained by applying virtual loads to the foundation model. The comparison of dynamic properties of models developed in SAP2000 and ANSYS softwares shows that this approach gives very good results. Also, the damping of the structure is included in the model by defining Rayleigh damping constants. Pushover analysis results show that the pushover curve remains almost perfectly linear before buckling as nonlinearity is seen in the last few steps before buckling. As the buckling occurs, a sudden drop is observed in the pushover curve of the tower. After the sudden drop, the capacity continues to decrease gradually. Also, the influences of considering initial imperfections and including the dead load of nacelle and hub parts are investigated. It is seen that including dead load decreases the buckling capacity of the tower remarkably. Also, it is observed that initial imperfections may lead to severe decreases in the buckling capacity of the structure therefore it is concluded that occurrences of initial imperfections should be monitored carefully.

The structural performance of the wind turbine is assessed by two different approaches. Firstly, the capacity curve of the wind turbine is obtained from the pushover curve. In this process, the pushover curve that considers dead load actions and ignores initial imperfection is used. Then, the demand curve is obtained from the design spectrum of the wind turbine site which is obtained from the Turkish Seismic Code. Finally, these two curves are compared, and the performance point is obtained which is the intersection point of two curves. At the performance point, spectral top displacement is found as 240 mm which is far below the top displacement level where the buckling occurs. So, it is concluded that the wind turbine is very safe against buckling under an expected earthquake level without any wind loading.

Also, seismic fragility analysis of the wind turbine is performed. In this scope, 4 different fragility curves are developed for considering different levels of wind loading.

In the incremental dynamic analyses used for the development of fragility curves, the buckling of the steel tower of the wind turbine is taken as the damage state. Analyses are performed for 11 different earthquake records which are compatible with the design spectrum of the wind turbine site. Fragility analysis shows that the spectral acceleration level causing the buckling of the steel tower is 1.8g for the parked condition which is unlikely to see in the wind turbine site. Also, it is seen that the fragility curve of the case considering wind loading with 5 m/s mean wind speed is very similar to the fragility curve of the parked condition which shows that the influence of the 5 m/s wind speed on the structural performance is very limited. However, the influence of wind loading becomes significant when the mean speed of the wind is equal to 15 m/s as the spectral acceleration level for the buckling of the steel tower decreases to 0.9g for this case. This is very important because 15 m/s wind speed equals approximately the rated wind speed at which the wind turbine produces electricity at its maximum capacity. So, it is seen that wind speed needed for the maximum electricity generation influences the structural performance of the wind turbine significantly and it is concluded that the wind load action definitely should be included in the assessment of the structural performance of wind turbines. Also, the spectral acceleration level for the buckling of the tower decreases to 0.8g for 25 m/s mean wind speed which shows that the capacity continues to decrease as the wind loading increases.

Also, the resonance phenomenon for wind turbine towers is studied. Possible sources of excitation arising from the rotation of blades and the possibility of the occurrence of resonance are discussed. The rotor speed level which is susceptible to cause resonance is obtained from the Campbell diagram. The Campbell diagram shows that resonance may occur due to mass unbalance therefore real-time acceleration records are examined, and the occurrence of resonance is investigated. In the real-time acceleration time histories, additional excitation which is expected to arise because of resonance is not seen at the resonance rotor speed levels. This shows that resonance does not occur on the wind turbine probably due to homogeneous mass distribution of three blades.

Finally, the buckling capacity of the wind turbine tower is calculated analytically according to two different references. When analytical buckling capacities are compared with moment demands obtained in time-history analyses, very good agreement is observed between capacity and demand values. This shows that analytical buckling capacities obtained according to these references are reasonable.

In future works, this study can also be improved by means of several different topics discussed below.

- The soil has dynamic properties that influence the soil-structure interaction. Even without a structure built on the soil, the soil has natural frequencies which may lead to resonance phenomenon under seismic action. In the case of building wind turbines which are tall structures and susceptible to experience rocking failures, the dynamic properties of the soil can become important in terms of resonance phenomenon. In our study, dynamic properties of the soil are ignored and soil flexibility is considered with soil springs which have static stiffnesses since the fundamental period of the wind turbine is very long and the modal participation factor of the first mode is high. Also, a piled foundation exists in the wind turbine investigated in our study which makes the probability of observing rocking motion in the structure very unlikely. But in future studies, the dynamic properties of the soil can be included in the model and its influence on the structural behavior of the wind turbine can be investigated in a detailed manner.
- In this study, elastic bucking analysis is performed to define initial imperfections to the model. In the future studies, an investigation for the possible sources of initial imperfections and the possible types of initial imperfections can also be investigated for wind turbines. For this purpose, a study for developing stochastic imperfection models can also be made.
- Also, the soil deposit of the wind turbine includes a sand layer and the location of the wind turbine is close to the Black Sea therefore the liquefaction phenomenon can also be important in the structural performance of the wind turbine. In our study, we ignored liquefaction probability of the soil since the location of the wind

turbine is not that close to the sea and the altitude of the wind turbine is high. But still, it can be considered in future studies and the influence of liquefaction on the structural behavior can be investigated.

REFERENCES

1. Asareh, M.-A., I. Prowell, J. Volz and W. Schonberg, "A computational platform for considering the effects of aerodynamic and seismic load combination for utility scale horizontal axis wind turbines", *Earthquake Engineering and Engineering Vibration*, Vol. 15, No. 1, pp. 91–102, 2016.

2. Asareh, M. A. and I. Prowell, "A simplified approach for implicitly considering aerodynamics in the seismic response of utility scale wind turbines", *53rd AIAA/ASME/ASCE/AHS/ASC Structures, Structural Dynamics and Materials Conference 20th AIAA/ASME/AHS Adaptive Structures Conference 14th AIAA*, p. 1829, 2012.

3. Valamanesh, V. and A. Myers, "Aerodynamic damping and seismic response of horizontal axis wind turbine towers", *Journal of Structural Engineering*, Vol. 140, No. 11, p. 04014090, 2014.

4. Eads, L., E. Miranda, H. Krawinkler and D. G. Lignos, "An efficient method for estimating the collapse risk of structures in seismic regions", *Earthquake Engineering & Structural Dynamics*, Vol. 42, No. 1, pp. 25–41, 2013.

5. Lavassas, I., G. Nikolaidis, P. Zervas, E. Efthimiou, I. Doudoumis and C. Baniotopoulos, "Analysis and design of the prototype of a steel 1-MW wind turbine tower", *Engineering Structures*, Vol. 25, No. 8, pp. 1097–1106, 2003.

6. Yang, J. N., Y. Xia and C.-H. Loh, "Damage identification of bolt connections in a steel frame", *Journal of Structural Engineering*, Vol. 140, No. 3, 2014.

7. Kiyomiya, O., T. Rikiji, P. H. van GELDER *et al.*, "Dynamic response analysis of onshore wind energy power units during earthquakes and wind", *The Twelfth International Offshore and Polar Engineering Conference*, International Society of

Offshore and Polar Engineers, 2002.

8. Staino, A. and B. Basu, "Dynamics and control of vibrations in wind turbines with variable rotor speed", *Engineering Structures*, Vol. 56, pp. 58–67, 2013.

9. Blachowski, B. and W. Gutkowski, "Effect of damaged circular flange-bolted connections on behaviour of tall towers, modelled by multilevel substructuring", *Engineering Structures*, Vol. 111, pp. 93–103, 2016.

10. Prowell, I., A. Elgamal, C. Uang and J. Jonkman, *Estimation of seismic load demand for a wind turbine in the time domain*, Tech. rep., National Renewable Energy Lab.(NREL), Golden, CO (United States), 2010.

11. Prowell, I., M. Veletzos, A. Elgamal and J. Restrepo, "Experimental and numerical seismic response of a 65 kW wind turbine", *Journal of Earthquake Engineering*, Vol. 13, No. 8, pp. 1172–1190, 2009.

12. Cao, J. and A. Bell, "Experimental study of circular flange joints in tubular structures", *The Journal of Strain Analysis for Engineering Design*, Vol. 31, No. 4, pp. 259–267, 1996.

13. Prowell, I., A. Elgamal and J. Jonkman, *FAST simulation of seismic wind turbine response*, Tech. rep., National Renewable Energy Lab.(NREL), Golden, CO (United States), 2010.

14. Sim, H.-B., I. Prowell, A. Elgamal and C.-M. Uang, "Flexural tests and associated study of a full-scale 65-kW wind turbine tower", *Journal of Structural Engineering*, Vol. 140, No. 5, p. 04013110, 2014.

15. Quilligan, A., A. O'Connor and V. Pakrashi, "Fragility analysis of steel and concrete wind turbine towers", *Engineering structures*, Vol. 36, pp. 270–282, 2012.

16. Prowell, I., M. Veletzos and A. Elgamal, "Full scale testing for investigation of

wind turbine seismic response", *CiteSeer*, 2008.

17. Drenick, C., I. Prowell, D. Dolan *et al.*, "In Depth Cost of Energy Analysis of East Coast Offshore Wind Farms", *Offshore Technology Conference*, Offshore Technology Conference, 2014.

18. Pollino, M. C. and A. A. Huckelbridge, "In-situ measurements of fatigue demands on a wind turbine support structure", *2012 IEEE Energytech*, pp. 1–5, IEEE, 2012.

19. Seidel, M. and P. Schaumann, "PG4. 1 Measuring Fatigue Loads of Bolts in Ring Flange Connections", *EWEC-CONFERENCE-*, pp. 255–258, 2001.

20. Prowell, I., T. Schmidt, A. Elgamal, C.-M. Uang, H. Romanowitz and J. E. Duggan, "Measuring global response of a wind turbine to simulated earthquake shaking assisted by point tracking videogrammetry", *52nd AIAA/ASME/ASCE/AHS/ASC Structures, Structural Dynamics and Materials Conference 19th AIAA/ASME/AHS Adaptive Structures Conference 13t*, p. 1946, 2011.

21. Nuta, E., C. Christopoulos and J. A. Packer, "Methodology for seismic risk assessment for tubular steel wind turbine towers: application to Canadian seismic environment", *Canadian Journal of Civil Engineering*, Vol. 38, No. 3, pp. 293–304, 2011.

22. Prowell, I., A. Elgamal and J. Lu, "Modeling the influence of soil structure interaction on the seismic response of a 5 MW wind turbine", *5th International Conference on Recent Advances in Geotechnical Earthquake Engineering and Soil Dynamics*, 2010.

23. Ishihara, T. and M. Sarwar, "Numerical and theoretical study on seismic response of wind turbines", *European Wind Energy Conference and Exhibition*, pp. 1–5, 2008.

24. Mensah, A., L. Duenas-Osorio, I. Prowell and M. Asareh, "Probabilistic combination of earthquake and operational loads for wind turbines", *Proceedings of the 15th World Conference on Earthquake Engineering, Lisbon, Portugal*, 2012.

25. Guo, L., C.-M. Uang, A. Elgamal, I. Prowell and S. Zhang, "Pushover analysis of a 53 m high wind turbine tower", *Advanced Science Letters*, Vol. 4, No. 3, pp. 656–662, 2011.

26. Stamatopoulos, G. N., "Response of a wind turbine subjected to near-fault excitation and comparison with the Greek Aseismic Code provisions", *Soil Dynamics and Earthquake Engineering*, Vol. 46, pp. 77–84, 2013.

27. Díaz, O. and L. E. Suárez, "Seismic analysis of wind turbines", *Earthquake Spectra*, Vol. 30, No. 2, pp. 743–765, 2014.

28. Hongwang, M., "Seismic analysis for wind turbines including soil-structure interaction combining vertical and horizontal earthquake", *Proceedings of the 15th World Conference on Earthquake Engineering, Lisbon*, 2012.

29. He, G., J. Li *et al.*, "Seismic analysis of wind turbine system including soil-structure interaction", *Proceedings of the 14th World Conference on Earthquake Engineering*, 2008.

30. Kafali, C. and M. Grigoriu, "Seismic fragility analysis", *9th ASCE Specialty Conference on Probabilistic Mechanics and Structural Reliability*, pp. 1–6, 2004.

31. Zhao, X. and P. Maisser, "Seismic response analysis of wind turbine towers including soil-structure interaction", *Proceedings of the Institution of Mechanical Engineers, Part K: Journal of Multi-body Dynamics*, Vol. 220, No. 1, pp. 53–61, 2006.

32. Kjørlaug, R. A., A. M. Kaynia and A. Elgamal, "Seismic response of wind turbines due to earthquake and wind loading", *Proceedings of the 9th International*

Conference on Structural Dynamics, EURODYN, pp. 3627–3634, 2014.

33. Prowell, I., M. Veletzos, A. Elgamal and J. Restrepo, "Shake table test of a 65 kW wind turbine and computational simulation", *14th World Conference on Earthquake Engineering, Beijing, China*, pp. 12–17, 2008.

34. Prowell, I., A. Elgamal, C.-M. Uang, J. Enrique Luco, H. Romanowitz and E. Duggan, "Shake table testing and numerical simulation of a utility-scale wind turbine including operational effects", *Wind Energy*, Vol. 17, No. 7, pp. 997–1016, 2014.

35. Prowell, I., C.-M. Uang, A. Elgamal, J. E. Luco and L. Guo, "Shake table testing of a utility-scale wind turbine", *Journal of Engineering Mechanics*, Vol. 138, No. 7, pp. 900–909, 2012.

36. Bazeos, N., G. Hatzigeorgiou, I. Hondros, H. Karamaneas, D. Karabalis and D. Beskos, "Static, seismic and stability analyses of a prototype wind turbine steel tower", *Engineering Structures*, Vol. 24, No. 8, pp. 1015–1025, 2002.

37. Patil, A., S. Jung and O.-S. Kwon, "Structural performance of a parked wind turbine tower subjected to strong ground motions", *Engineering Structures*, Vol. 120, pp. 92–102, 2016.

38. Robertson, A. N., J. M. Jonkman, A. J. Goupee, A. J. Coulling, I. Prowell, J. Browning, M. D. Masciola and P. Molta, "Summary of conclusions and recommendations drawn from the DeepCwind scaled floating offshore wind system test campaign", *ASME 2013 32nd International Conference on Ocean, Offshore and Arctic Engineering*, American Society of Mechanical Engineers Digital Collection, 2013.

39. Haenler, M., U. Ritschel and I. Warnke, "Systematic modelling of wind turbine dynamics and earthquake loads on wind turbines", *European Wind Energy Conference and Exhibition*, pp. 1–6, Citeseer, 2006.

40. Drenick, C., I. Prowell and D. Dolan, "The Effect of Wind Data Resolution on the Predicted Energy Generation of an Offshore Wind Farm", *ASME 2014 33rd International Conference on Ocean, Offshore and Arctic Engineering*, American Society of Mechanical Engineers Digital Collection, 2014.

41. Kjørlaug, R. A. and A. M. Kaynia, "Vertical earthquake response of megawatt-sized wind turbine with soil-structure interaction effects", *Earthquake Engineering & Structural Dynamics*, Vol. 44, No. 13, pp. 2341–2358, 2015.

42. Bozorgnia, Y., S. A. Mahin and A. G. Brady, "Vertical response of twelve structures recorded during the Northridge earthquake", *Earthquake Spectra*, Vol. 14, No. 3, pp. 411–432, 1998.

43. Hu, W.-H., S. Thöns, R. G. Rohrmann, S. Said and W. Rücker, "Vibration-based structural health monitoring of a wind turbine system. Part I: Resonance phenomenon", *Engineering Structures*, Vol. 89, pp. 260–272, 2015.

44. Katsanos, E. I., S. Thöns and C. T. Georgakis, "Wind turbines and seismic hazard: a state-of-the-art review", *Wind Energy*, Vol. 19, No. 11, pp. 2113–2133, 2016.

45. API, "Recommended practice for planning, designing and constructing fixed offshore platforms–working stress design–", *American Petroleum Institute Recommended Practice RP2A-WSD*, 2000.

46. Matlock, H., "Correlations for design of laterally loaded piles in soft clay", *Offshore Technology in Civil Engineering's Hall of Fame Papers from the Early Years*, pp. 77–94, 1970.

47. FineSoftware, "Friction Angle on Pile Skin", `https://www.finesoftware.eu/help/geo5/en/friction-angle-on-pile-skin-01/`, last accessed on 14/07/2020.

48. Hanbay, S., *Vibration-Based Structural Health Monitoring of a Wind Turbine In-*

corporating Environmental and Operational Conditions, Master's Thesis, Boğaziçi University, 2019.

49. Chopra, A. K., *Dynamics of Structures, Theory and Applications to Earthquake Engineering, 4th Ed*, 2012.

50. Shinozuka, M., M. Feng, H. Kim, T. Uzawa and T. Ueda, *Statistical Analysis of Fragility Curves*, Tech. rep., Technical Report MCEER, 2001.

51. Jonkman, B. J., *TurbSim user's guide: Version 1.50*, Tech. rep., National Renewable Energy Lab.(NREL), Golden, CO (United States), 2009.

52. Jonkman, J. M., M. L. Buhl Jr *et al.*, *FAST user's guide*, Tech. rep., National Renewable Energy Lab.(NREL), Golden, CO (United States), 2005.

53. Center, S. P., "Beaufort Wind Scale", `https:https://www.spc.noaa.gov/faq/tornado/beaufort.html`, last accessed on 20/07/2020.

54. Kalan, O., *Fatigue Life Assessment of 5 MW Onshore Wind Turbines*, Master's Thesis, Boğaziçi University, 2012.

55. Gasch, R. and J. Twele, *Wind Power Plants: Fundamentals, Design, Construction and Operation*, Springer Science & Business Media, 2011.

56. Niebsch, J., R. Ramlau and T. T. Nguyen, "Mass and aerodynamic imbalance estimates of wind turbines", *Energies*, Vol. 3, No. 4, pp. 696–710, 2010.

57. AISC, "Specification for structural steel buildings", *American Institute of Steel Construction, Chicago, IL*, 2016.

58. Ziemian, R. D., *Guide to Stability Design Criteria for Metal Structures*, John Wiley & Sons, 2010.